PONTIFICIA UNIVERSIDAD CATÓLICA DEL PERÚ

ESCUELA DE POSGRADO

On the fundamental absorption of amorphous semiconductors

Student:
Jose Ruben Angulo Abanto

Advisor:

Mg. Jorge Andrés Guerra Torres

Committee:
Dr. Roland Weingärtner
Dr. Jan Amaru Palomino Töfflinger

Lima, February 2016

Abstract

The present thesis reviews different models that describe the fundamental absorption of amorphous semiconductors. These models make use of the electronic density of states to shape the absorption coefficient in the fundamental absorption region. The study focuses on the optical absorption of hydrogenated amorphous Silicon (*a*-Si:H), hydrogenated and non-hydrogenated amorphous silicon carbide (*a*-SiC:H_x), and silicon nitride (*a*-SiN) thin films. On the one hand, parameters like the Tauc-gap and Urbach energy are obtained from the absorption coefficient using the traditional models. On the other hand, a recently proposed model based on band thermal fluctuations was assessed [1]. This model allows a determination of the mobility gap and the Urbach energy from a single fit of the absorption coefficient without the need of identifying the Tauc region beforehand. Furthermore, it is able to discriminate the variation of the Urbach energy from the bandgap. The results allow the evaluation of the aforementioned parameters with annealing treatments at different temperatures. The mobility edges are insensitive to the structural disorder by at least one degree lower than the Urbach energy. This work demonstrates that it is possible to obtain the mobility edge through this model. In addition, the measured Tauc-gap and Urbach energy exhibit a strong linear correlation following the Cody model for all three materials. Finally, the Urbach focus concept is evaluated and estimated under different analysis.

Resumen

En la presente tesis se revisan los diferentes modelos que describen la absorción fundamental de los semiconductores amorfos. Estos modelos hacen uso de la densidad de estados electrónicos para la forma del coeficiente de absorción en la región fundamental de absorción. El estudio se centra en la absorción óptica de películas delgadas de silicio amorfo hidrogenado (*a*-Si:H), carburo de silicio hidrogenado y sin hidrogeno amorfo *a*-SiC:H_x y nitruro de silicio amorfo *a*-SiN. Se obtuvieron parámetros como el Tauc-gap y la energía Urbach. Luego, se probó un modelo propuesto recientemente que considera las fluctuaciones térmicas de la banda. Este modelo permite determinar la brecha de los bordes de movilidad y la energía Urbach aplicando un solo ajuste del coeficiente de absorción sin la necesidad de la identificación de la región Tauc y Urbach de antemano. Además, es capaz de discriminar la variación de la energía de Urbach en banda prohibida. Los resultados permiten la evaluación de los parámetros antes mencionados, con el recocido de los tratamientos a diferentes temperaturas. Tomando ventaja que los bordes de movilidad deben permanecer insensible al desorden estructural (al menos en un grado menor que la energía Urbach) este trabajo demuestra que es posible obtener el borde movilidad a través de este modelo. Además, la medida Tauc-gap y la energía Urbach mostraron una fuerte conexión reproduciendo la relación lineal de Cody para los tres materiales. Por último, el concepto del foco Urbach se evalúa y se estima por diferentes análisis como son: ajuste global, relación lineal de Cody, análisis de Orapunt y nuestra aproximación.

Acknowledgments

This research has funded by the National Council of Science and Technology (CONCYTEC) under the agreement PUCP-FONDECYT 012-2013. My supervisor Mg. Jorge Andrés Guerra has enabled me to pursue my studies to the best of my ability. His guidance and support have been unparalleled. I would like to acknowledge and express my gratitude and thanks to Prof. Dr. Roland Weingärtner for accepting me in his laboratory. Additionally, I like to acknowledge my colleagues, Liz Montañez and Alvaro Tejada in the Solid State Physics Group at the PUCP who provided me with the samples and supported me with the measurements.

Contenido

1. Introduction

Knowledge of the absorption coefficient is especially important in the design and analysis of solid state devices. In this sense, the optical absorption in amorphous semiconductors has been one of the central objectives to understand the electronic processes [2][3]. The analysis of optical data of amorphous semiconductors is usually subjected to unsuitable models. For instance, the Tauc-model does not take into account tail-tail and band-tail electronic transitions. Tail states in amorphous semiconductors overlap on the fundamental absorption region. Therefore, the possibility to obtain information from the absorption coefficient on the optical bandgap and electronic density of states is often overlooked [4]. Thereby, the aim is to develop an understanding of the optical response of amorphous semiconductors over the fundamental absorption spectral range.

In 1953, Urbach showed experimentally an exponential tail absorption that increased with the incident photon [6]. Additionally, in 1966, Tauc et. al. studied the optical properties of amorphous germanium [5]. In his study Tauc proposed a simple model for the fundamental absorption of amorphous semiconductors. Since then, a large number of amorphous semiconductors has been studied under the Urbach and Tauc models [7]. Then, most empirical density of states models have been built upon disordered semiconductor phenomenology [8][9].

Other models follow the assumption that a disordered material can be studied as an ordered one at high temperature (frozen phonon model) [1][10][11]. Here, our goal is to establish a clear characterization of the optical absorption spectrum by different analysis. It have been included the classical models, Tauc and Urbach, and a new one herein named Guerra's model [1][12]. This work focuses on studying the optical properties of three relevant materials, which present a variation of the disorder degree after annealing treatments. The first material is hydrogenated amorphous silicon (*a*-Si: H). This material is used in several applications, such as active matrix displays [13], thin film transistors [14], photodiodes [15] and heterojunction solar cells [16][17].

The second material is hydrogenated amorphous silicon carbide (*a*-SiC: H_x). This material is of interest for several electronic applications [18]. For instance: in optoelectronic devices, such as heterojunction solar cells [19], devices for light emission [20], thin film transistors [21] and photodiodes [22][23]. The third material is silicon nitride. This material has been used in the design of advanced solar cells [24]. Furthermore, it can be used as protective overcoats on magneto optical films. Moreover, SiN thin films play an important role for the passivation of silicon [25].

The present thesis is organized in the following manner. In sections 2.1 and 2.2, it introduces the optical absorption by electronic processes in the crystalline case. Thereby, it studies the structure and highlights the main differences of the amorphous case. The objective is to review briefly how the optical response of amorphous materials behaves by measuring the optical absorption coefficient and studying its variations after annealing treatments. In section 2.3, a brief review of the empirical density of states models, that have been developed for the analysis of the optical properties of disordered semiconductors, is presented [10]. The new model proposed by Guerra et al[1] is shown and deliver some insights on the Urbach focus concept. Finally, in the section 3, a comparison is performed between the new model with the traditional ones.

2. Fundamental theory

2.1 Background

The quantum mechanics allow us understanding the properties of semiconductors. To begin, some of the most basic concepts and principles will be introduced that allow us to recognize and describe the optical absorption process. In this way, it is instructive to start with the crystalline structure. Thenceforth, the Bloch's theorem can be deduced taking advantage of the periodical arrangement of atoms. On the other hand, the main feature in amorphous is that there is no long range periodicity. Finally, the different approaches to shape the electronic density of states for the quasifree electron case in order to understand and model the absorption process is considered.

2.1.1 Crystals

The physical properties of any material are linked to the solid state structure and the electronic process that take place under certain excitations. A crystalline solid is a large group of atoms that bond one another so as to confine the atoms to a definite volume of space. Additionally, the crystal presents a periodic array of atoms or ions throughout the whole solid [26]. Formally, it is applied the concept of unit cell and a set of vectors **R** (lattice vectors). Now, by translation operators, it is able to generate the crystalline lattice (see Figure 2.1). The lattice vectors are given by

$$R = a_1\vec{a} + a_2\vec{b} + a_3\vec{c}$$

Where $\vec{a}, \vec{b}, \vec{c}$ are the linearly independent vectors, a_1, a_2, a_3 are number positive or negative and integer values. An ideal crystal has infinite translation symmetry in all three dimensions and as a consequence, it presents a long range order.

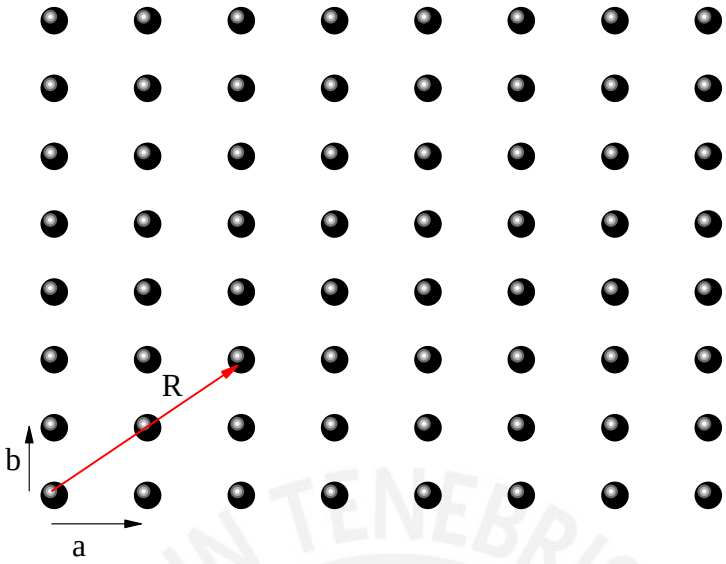

Figure 2.1 A schematic depiction of the distribution of atoms or ions within equilibrium position in an ideal crystal

In one sense, the atoms have a regular array and in their equilibrium positions. However, at any given temperature, the atoms may vibrate with small amplitudes about their fixed equilibrium positions. It has been considered only perfect crystalline solids, but defects and the temperature effect will be introduced later for modeling amorphous materials by perturbation of the equilibrium position.

2.1.2 Bloch's theorem

The Bloch theorem is a consequence of the periodicity of the crystalline lattice [27]. Electrons and holes can be described by wavefunctions which are extended in space with quantum states defined by the momentum ***k***. The Bloch function is the product of an envelope function ($e^{ik.r}$), that describes the global behavior, and a unit cell function (u_k) [28].

$$|r,k\rangle = u_k(r)e^{ik.r} \qquad \textit{Equation 2.1}$$

Where $u_k(r) = u_k(r) + u_k(r+R)$, it is periodic. Thereby, it has the fundamental translational symmetry of the crystal. Bloch's theorem tells us that it is possible always choose the crystalline wave functions to be not localized.

2.1.3 Amorphous structure

An ideal crystal presents an atomic arrangement that has infinite translation asymmetry in all three dimensions. On the contrary, amorphous materials, exhibit a lack of order in their atomic structure. In consequence, the wave vector ***k*** is no longer a good quantum number, thereby the energy bands cannot be described by the E-***k*** dispersion relation. Nevertheless, the short range order is still present. Hass and Ehrenreich have shown that both, amorphous and crystalline, structures have the same local symmetry [29]. Now, there are different theoretical approaches to model the optical properties in amorphous materials [4].

A real crystal presents a finite size and different types of defects such as vacancy, interstitial and dislocation in the network. Which means that in a real crystal the translation symmetry is not fully kept [30]. On the other hand, amorphous materials present: dangling bonds, different bond length, bond angles and it presents different coordination numbers at individual atomic sites, see Figure 2.2.

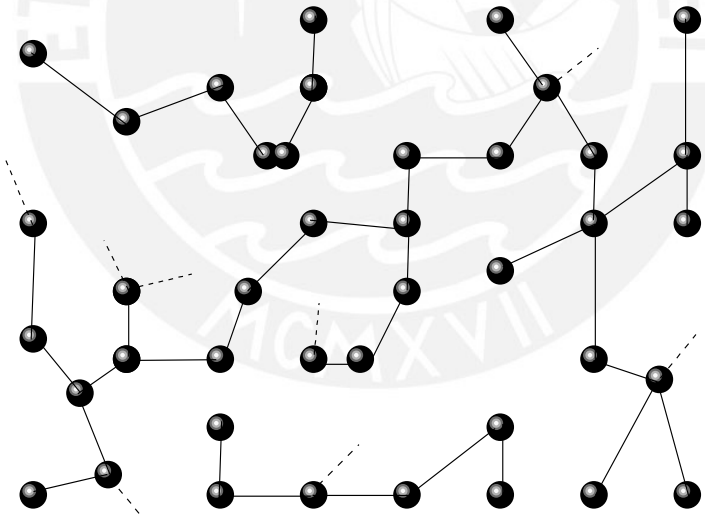

Figure 2.2 Amorphous structure

The disordered structure has the effect to cause scattering causing wavefunction misses the phase coherence over a distance due that the potential is not periodic and results in small perturbation the wave function of electronic state then in amorphous materials are present extended state and localized state. In section 2.3 will be discussed

2.1.4 Density of states in the quasifree-electron approximation

The density of states give us another starting point for discussing the solid state properties. An electron in a solid presents a little different from a free electron since between the valence electron and network present the weakly interaction. Then, it is convenient to assign a quasifree electron with effective mass m^*, it is a definition using the host matrix atoms with periodic potential. According to quantum mechanics the Schrödinger's equation

$$-\frac{\hbar^2}{2m^*}\nabla^2 \left| r,k\right\rangle = E\left| r,k\right\rangle \qquad \textit{Equation 2.2}$$

Here $\hbar$ is thePlanck's constant, $\left| r,k\right\rangle$is the wavefunctions associated an electron, ∇^2 represents the mathematical operator $\frac{\partial^2}{\partial x^2}+\frac{\partial^2}{\partial y^2}+\frac{\partial^2}{\partial z^2}$, the wavefunctions associated an electron $\left| r,k\right\rangle = \sqrt{V}^{-1}\exp(e\boldsymbol{k}.r)$, and following procedure for the solution of Schrödinger's equation and defined the density of state as is the number de states per energy per volume. It could be written the density of states in the quasifree electron approximation [28]

$$D(E) = \sqrt{2}\frac{m^{*3/2}}{\pi^2\hbar^3}(E)^{1/2} \qquad \textit{Equation 2.3}$$

If the spin of electron was included, the Equation 2.3 is then multiplied by 2. It is important to mention that the Equation 2.3 is most often used with Fermi–Dirac distribution, $f(E_c)$, which express the average number of electrons per state at a determinate temperature $D\ (E)\times f(E_c)dE$.

In the formation of energy bands is a consequence of bonding and anti-bonding orbitals states. Under the quasifree electron approximation (section 2.1.4), the density of states for valence and conduction band, can be written as [28]:

$$D_c(E_c) = \sqrt{2}\frac{m_h^{*3/2}}{\pi^2\hbar^3}\sqrt{E_c - E_c(0)} \qquad \textit{Equation 2.4}$$

$$D_v(E_v) = \sqrt{2}\frac{m_e^{*3/2}}{\pi^2\hbar^3}\sqrt{E_v(0) - E_v}$$

Here $m^*_{e/h}$ is the hole and electron effective mass, respectively. $E_c(0)$ and $E_v(0)$ are arbitraries constants. Figure 2.3 depicts the two bands separated by an energy gap $E_g = E_c(0) - E_v(0)$.

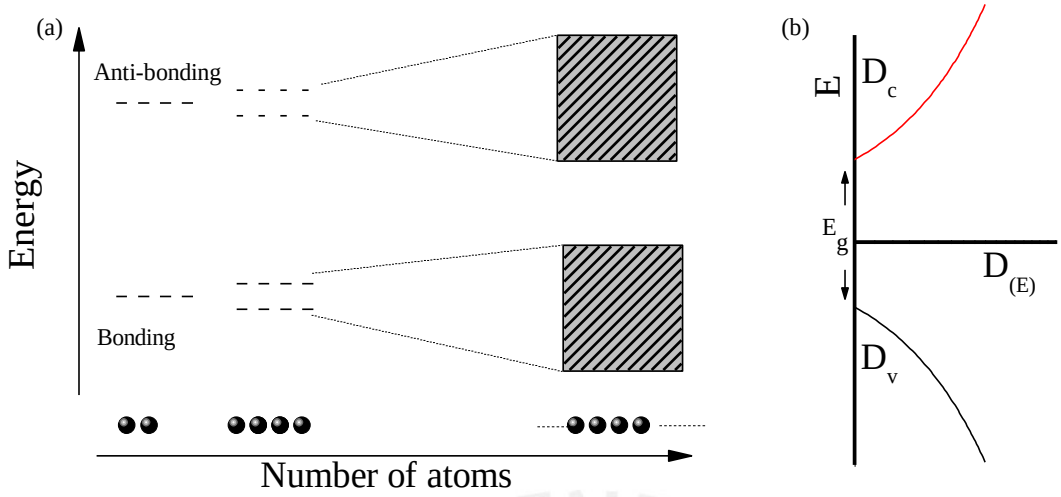

Figure 2.3 (a) Bonding and anti-bonding state, (b) Density of state in valance and conductions, under the quasifree electron approximation

Finally, the existence of energy bands is not a consequence of the translational symmetry nor the fact that they are separated by an energy gap. Additionally, the energy gap depends on the inter-atomic distance [31].

2.2 Fundamental absorption in crystalline semiconductors

The fundamental absorption edge contains information of the electronic structure of the material. Therefore, the purpose of this section is to review the fundamental absorption calculation in the crystalline case. The optical properties of solids are associated to the interaction of solids with electromagnetic radiation whose wavelength ranges from the infrared to the ultraviolet. There are several processes involved in absorption. The optical absorption in the UV-VIS-NIR is mainly due to electronic transitions between the valence and conduction bands of semiconductors. To begin, the absorption process is studied by perturbation theory. Then, the electromagnetic field is described by a vector potential $\boldsymbol{A}$ and the scalar potential $\boldsymbol{\phi}$. In this sense, the Hamiltonian is written as:

$$\mathrm{H} = \frac{1}{2m}[p + e\boldsymbol{A}]^2 - e(\boldsymbol{\phi} + V) \qquad \text{Equation 2.5}$$

Here, e is the electron charge, p is the electron momentum, m is the electron mass and V is the potential in absence of an electromagnetic field. Moreover, the Coulomb gauge to describe the electromagnetic field, that is $\phi = 0, \nabla . A = 0$, and the electric and magnetic field are given by

$$E = -\frac{\delta A}{\delta t}, B = \nabla \times A \qquad \text{Equation 2.6}$$

Then, expanding Equation 2.5 and making an approximation such as it was ignore the quadratic terms in A, they are normally small compared to the linear terms in A. Additionally, the Coulomb gauge can be commuted, $[\mathrm{p}. A] = 0, \nabla . A = \mathrm{A}. \nabla$. Thereby, the Hamiltonian can be written:

$$\mathrm{H} = \frac{1}{2m} p^2 - eV + \frac{e}{m} A . p \qquad \textit{Equation 2.7}$$

Now, Fermi's golden rule was taken into account, then, the transition probability from the valance and conduction band by photon absorption per unit time per unit volume due to perturbation of the photon energy incident on the solid, H_{ER}. Then, the rate becomes[31]

$$R_{cv} = \frac{2\pi}{\hbar}\left(\frac{\mathbf{E}\, e}{2\omega m_e}\right)^2 \sum_{k_c, k_v} |M_{cv}|^2 \delta(E_c - E_v - \hbar\omega)\delta_{k_c, k_v} \qquad \textit{Equation 2.8}$$

Where m_e is the electron mass, e the electron charge, ω the photon frequency, $E_c$and E_c are the electron energy, $\boldsymbol{k_c}$ and $\boldsymbol{k_v}$the electron wave vector at the conduction and valence states. Transition matrix element in dipole approximation given by $|M_{cv}|e/m_e = \langle c|H_{eR}|v\rangle$

2.2.1 Direct and indirect materials

Let us now look the absorption coefficient using the Equation 2.8. In this sense, the power per unit volume lost is related the transition probability per unit volume R multiplied by the energy of each photon energy $\omega\hbar$. Additionally, the intensity of incident beam **I** decrease with the rate $-dI/dt$. Then, the power ratio loss equal:

$$R\omega\hbar = -\frac{dI}{dt} \qquad \textit{Equation 2.9}$$

For the case of light normally incident on a materials and in the absence of any reflection (see Figure 2.4). Light attenuation in intensity as it propagate through a material. For monochromatic light, in intensity of light diminishes exponentially as it pass through a material. Then, the Lambert-Beer law is given by

$$I = I_0 e^{-\alpha x} \qquad \textit{Equation 2.10}$$

Where I_0 denotes the intensity at the surface of the material, α is the optical absorption coefficient.

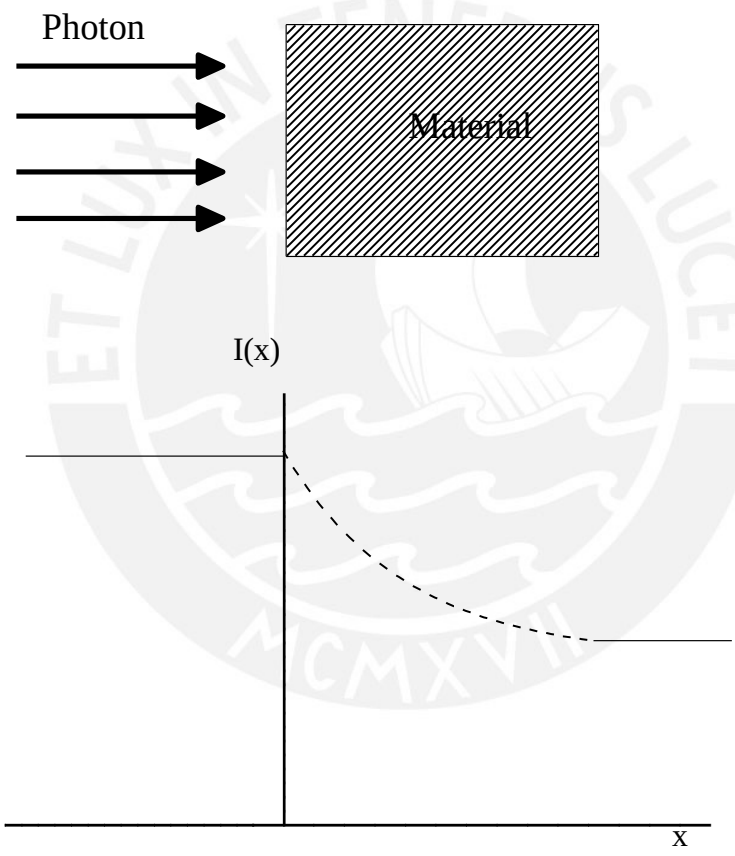

Figure 2.4 Light normally incident on a material

This coefficient describes the rate at which this exponential attenuation occurs and analysis the optical response of these materials when variation of the photon energy. Our study center in α being that allows for the quantitative prediction of the device performance. In reference to the Equation 2.10 is given by

$$-\frac{dI}{dt} = -\left(\frac{dI}{dx}\right)\left(\frac{dx}{dt}\right) = \frac{c}{n}\alpha I \implies R\omega\hbar = \frac{c}{n}\alpha I \qquad \textit{Equation 2.11}$$

Furthermore, the intensity, I, can be related to the field amplitude by

$$I = \frac{n^2}{8\pi}\left|E_{(\omega)}\right|^2 \qquad \textit{Equation 2.12}$$

The power loss from the field can also be expressed in terms of absorption coefficients α. Then, from the Equation 2.8, Equation 2.11 and Equation 2.12

$$\alpha = \frac{\hbar}{4\pi\epsilon_0 nc}\left(\frac{2\pi e}{m_e}\right)^2 \frac{1}{\hbar\omega}\sum_{k_c,k_v}|M_{cv}|^2\delta(E_c - E_v - \hbar\omega)\delta_{k_c,k_v} \qquad \textit{Equation 2.13}$$

Where $|M_{cv}|^2$ varies slowly with the photon energy, δ relate with the energy conservation and momentum in direct absorption process. Furthermore, the summation over the vector k can be written as a summation over the energy due to energy bands dispersion relation. These summation can be also calculated by the density of states [31]

$$\sum_k = \sum_E \Rightarrow \int D_{(E)}dE \qquad \textit{Equation 2.14}$$

Notice for direct optical transition, $k_c = k_v$ or $\delta_{k_c,k_v} = 1$. See Figure 2.5. it is defined E_{CV} as

$$E_{CV} = E_g + \frac{\hbar^2 k^2}{2\mu} \qquad \textit{Equation 2.15}$$

Where $E_{CV} = E_C - E_V$, E_g is the optical bandgap, and μ the reduced mass, $\mu^{-1} = m_e^{-1} + m_h^{-1}$. the Joint density of state JDOS is introduced as

$$J(E_{cv}) = \sqrt{2}\frac{\mu^{3/2}}{\pi^2\hbar^3}\sqrt{(E_{cv} - E_g)} \qquad \textit{Equation 2.16}$$

The matrix element change slowly with **k** and the Joint density state per unit volume to represent a summation over the energy.

$$\alpha = \frac{\hbar}{4\pi\epsilon_0 nc}\left(\frac{2\pi e}{m_e}\right)^2 \frac{1}{\hbar\omega}|M_{cv}|^2\int J(E_{cv})\delta(E_{cv} - \hbar\omega)dE_{cv} \qquad \textit{Equation 2.17}$$

Therefore, after integrating the Equation 2.17 the absorption coefficient for direct transitions is given by

$$^{dir}\alpha_{(\hbar\omega)} = M_{dir}^{1/2}\frac{\left(\hbar\omega - E_g\right)^{1/2}}{\hbar\omega}$$ *Equation 2.18*

Where M_{dir} contains all other constants. In contrast, for the case of indirect transition, the phonon assistance is considered ($k_c \neq k_v$), In such case, the maximum energy of the valence band and the minimum energy of the conduction band do not appear at the same ***k*** vectors, one has what is called an indirect bandgap semiconductor, see Figure 2.5. Moreover, the Fermi's Golden rule for indirect transitions look a bit different. The electronic transition matrix element includes the phonons.

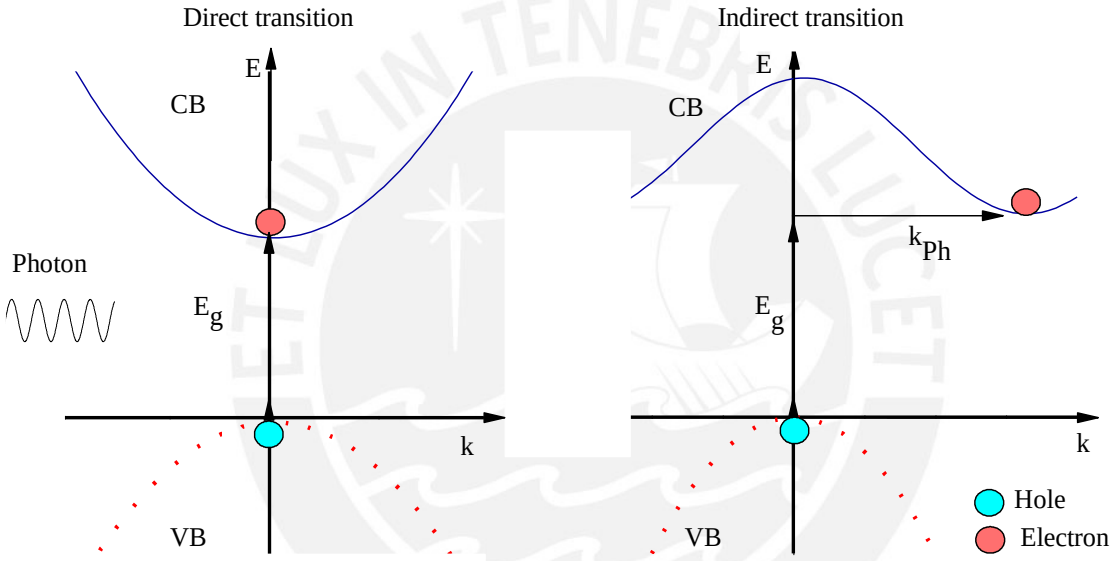

Figure 2.5Direc and indirect transition showing the most probable transitions

The indirect process as a two process in which the electron absorbs a photon and changes state then absorbs or emits a phonon.

2.3 Fundamental absorption in amorphous semiconductors

In a crystalline semiconductor, the conduction band and valence band distributions of states terminate clearly at their respective band edges. This leads to a well-defined bandgap (the minimum necessary energy to excite an electron from band to band, section 2.2.1. On the contrary, in an amorphous semiconductor, the distributions of conduction band and valence band states do not terminate clearly at the band edges, instead, the distributions of states invade into

the gap region. These states arise as a consequence of the disorder which characterizes these materials. The tail states are often associated as: variations in the bond lengths, bond angles, defects intrinsic, dangling bonds and vacancies [32]. Moreover, in the disorderless case, the wavefunctions are associated with the extended states, which are extended throughout the entire of the volume of the crystalline materials. In contrast, the tails are localized states. That is, the wavefunctions are confined to a small volume. The border region between the localized states and the delocalized states is called the mobility edge. A schematic representation of the electronic DOS distribution is plotted in Figure 2.6.

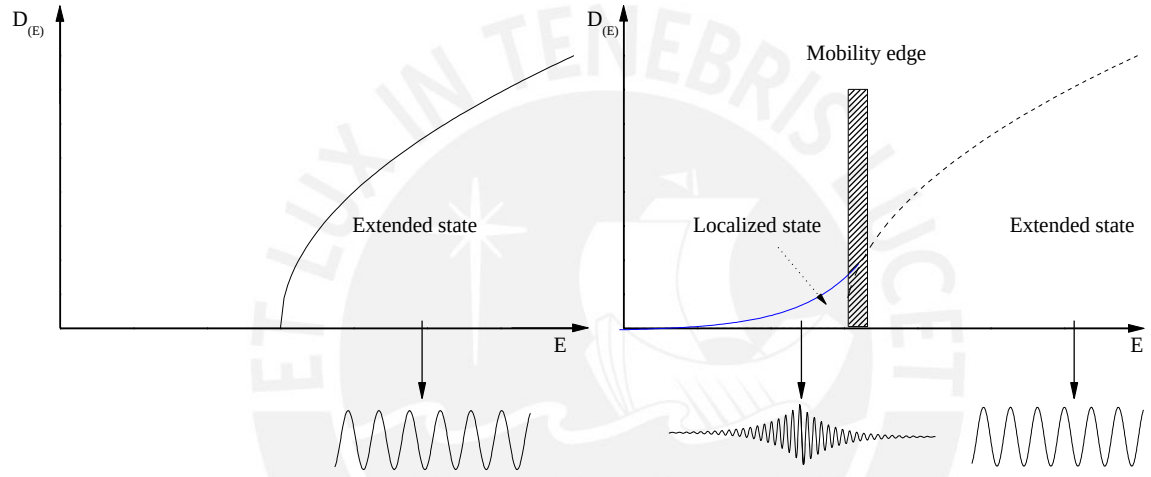

Figure 2.6 Schematic representation of the distribution of electronic states associated with a) Ideal crystalline, b) amorphous materials. The wavefunction associated localized state, in tail, and extended state are represented bellow.

The aim of the present thesis is to review existing models and to test a new model to describe the optical absorption coefficient. Figure 2.7 exhibits the typical shape of the absorption coefficient in the UV-VIS-NIR spectral region. It presents three principal zones: the very low absorption region arises from transitions involving defect states within the gap. In contrast, the mid absorption region exhibits an exponential behavior. This region is known as Urbach region, it arises from tail states. Finally, the strong absorption edge correspond to the fundamental absorption or Tauc region and corresponds to the band-to-band electronic transitions.

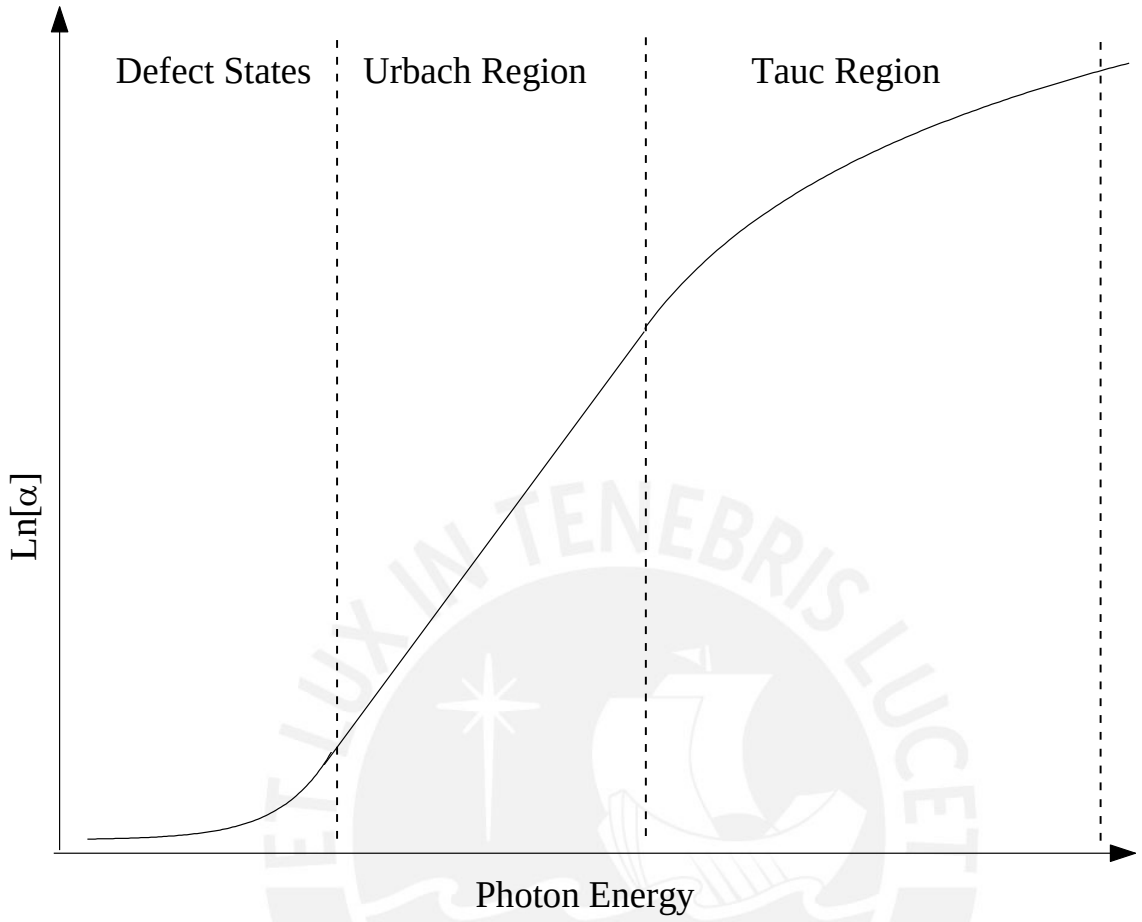

Figure 2.7 Three principal regions of the optical absorption in an amorphous semiconductor

In order to study the optical properties associated with amorphous semiconductors, from the absorption coefficient spectra. As it was seen previously, the shape of the absorption coefficient is directly related to the shape of the electronic density of states. Typically, in order to model the fundamental absorption of amorphous materials different models of the density of states have been developed. Here a brief review of these models is presented. First with the Tauc model because it introduces the bases in amorphous materials. In this case, the conservation of momentum does not apply to optical transition since the long-range order is not present and **k** is not a good quantum number. Additionally, it is important to remark that in the amorphous case a direct or indirect transition cannot distinguished.

2.3.1 Review of the electronic density of states models

The dependence of the absorption coefficient with the photon energy contains information of the electronic structure. Besides, the shape of the valance and conduction bands play a determining role on the optical absorption coefficient. In this sense, many authors proposed empirical models for valence and conduction band-edge in amorphous materials. Brief summaries of these models have been included. Different interpretation about the density of states and the empirical models will be given.

In 1966, Tauc et. al. [5] studied the optical properties of amorphous germanium. In this study Tauc proposed a simple model for density of state of amorphous semiconductors (see Equation 2.19).Tauc proposed to relax the conservation of momentum **k**. Furthermore, Tauc considered that the atomic arrangement in an amorphous solid as a perturbed lattice of the corresponding crystal and assumed that the density of states are the same in valance and conduction bands [5]

$$D_v(E) = C_1 \begin{cases} 0, & E > E_v \\ \sqrt{E_v - E}, & E \leq E_v \end{cases}$$

$$D_c(E) = C_2 \begin{cases} \sqrt{E - E_c}, & E \geq E_c \\ 0, & E < E_c \end{cases}$$

Equation 2.19

Here C_1, C_2 are constants, E_v, E_c are the valance and conduction band edges. This model has been widely used to find the optical bandgap in amorphous materials. The optical bandgap calculation will be discussed in section 2.3.3. Furthermore, O'Leary et al [33] proposed a generalization of the Tauc model by introducing the disorder characteristics of amorphous semiconductors through fluctuations around band edges as an average with a Gaussian distribution.

In 1980, Chen [8] investigated the thermalization gap E_T in hydrogenated amorphous silicon by photoluminescence excitation. In this work, they found for the emission of photons with an energy lower than the thermalization gap (<1.8 eV) by electron-hole radiative recombination and with a red-shifted in the spectrum. Chen et. al [8] constructed an empirical model by introducing an exponential density of states in the valance band for $E > E_v$. Additionally, Chen applied the Tauc model for $E \leq E_v$.

$$D_v(E) = \begin{cases} C_1 \exp\left(\frac{E_v - E}{\theta_v}\right), & E > E_v \\ C_2\sqrt{E_v - E_t - E}, & E \leq E_v \end{cases}$$

$$D_c(E) = C_3 \begin{cases} \sqrt{E - E_c}, & E \geq E_c \\ 0, & E < E_c \end{cases}$$

Equation 2.20

Here C_1, $C_2$and C_3 are constants, E_v, E_c are the valance and conduction band-edges, respectively. Chen et. al. concluded that in hydrogenated amorphous silicon, it is possible to define three energy gaps. The thermalization gap by excitation photoluminescence E_T, the optical gap by the Tauc model and the mobility gap.

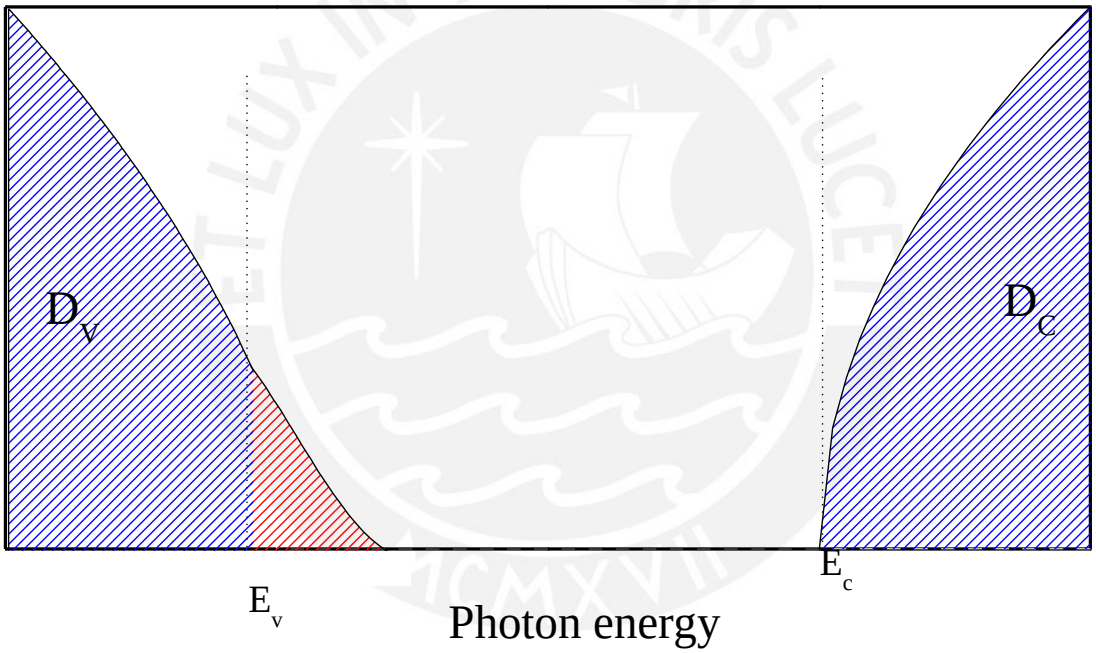

Figure 2.8 The empirical model of density of states considered by Chen et. al [8]

In 1982, Redfield [9] investigated the absorption edge of *a*-Si:H and found that the drift mobility of electrons and holes presented two band tails in the gap. They inferred that the energy dependence of both, valance and conduction bands tails, is exponential. Redfield considered three possible optical transitions: i) valence band to tail state in the conduction band, ii) valence band tail to the conduction band tail and iii) the valence band tail to the conduction band. However, it assumes horizontal distributions of valance band for $E \leq E_v$ and conduction band for $E \geq E_c$.

$$D_v(E) = C_1 \begin{cases} \exp\left(\frac{E_v - E}{\theta_v}\right), & E_v < E < E_c \\ 1, & E \leq E_v \end{cases}$$

$$D_c(E) = C_2 \begin{cases} 1, & E \geq E_c \\ \exp\left(\frac{E_v - E}{\theta_c}\right), & E_v < E < E_c \end{cases}$$

Equation 2.21

Here C_1 and C_2 are constants, $E_v$and E_c are valance and conduction band edges, θ_v and θ_c breadth of the valence and conduction tail. It is possible that breadth of the valence tail is equal to breadth of the conduction tail. The effect of these breadths are usually overlapped in the Urbach tail observed in the absorption coefficient.

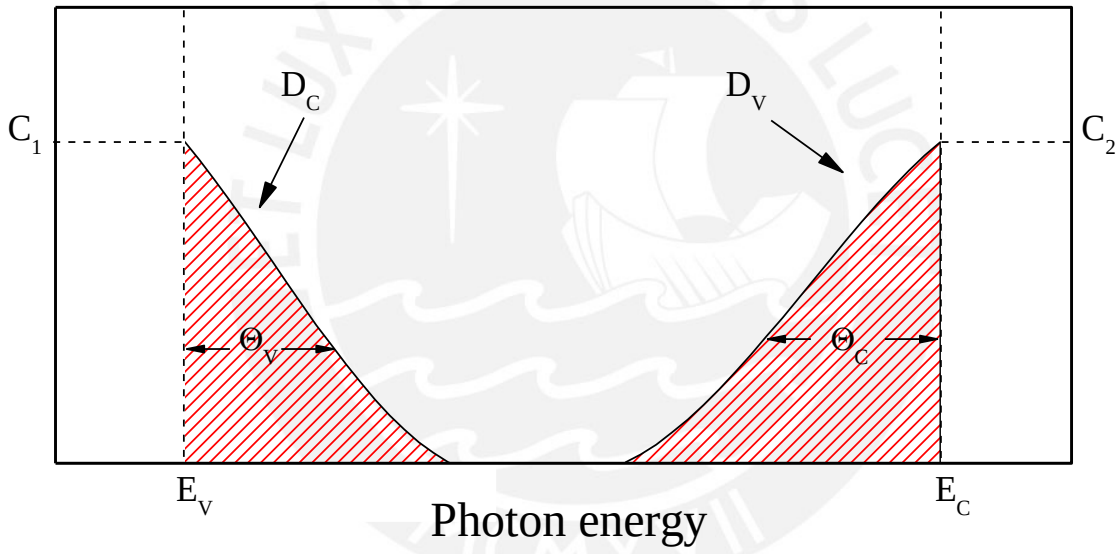

Figure 2.9 The empirical model of density of states considered by Redfield et. al. [9]

In 1984, Cody et. al. [34] introduced an exponential tail absorption by modifying the valance band edge (see Equation 2.22). Following the ideas of Chen et. al [8]. Furthermore, they considered that the parabolic and exponential density of states are continuous in the mobility energy $E_v - \frac{3\theta_v}{2}$ which denotes the transition point between square-root and linear-exponential distributions of states. They considered electronic transitions between valence band to conduction band and valence band tail to conduction band.

$$D_v(E) = C_1 \begin{cases} \sqrt{\frac{3\theta_v}{2}} \exp\left(-\frac{3}{2}\right) \exp\left(\frac{E_v - E}{\theta_v}\right), & E > E_v - \frac{3\theta_v}{2} \\ \sqrt{E_v - E}, & E \leq E_v - \frac{3\theta_v}{2} \end{cases}$$

Equation 2.22

$$D_c(E) = C_2 \begin{cases} \sqrt{E - E_c}, & E \geq E_c \\ 0, & E < E_c \end{cases}$$

Here C_1, C_2 are constants, $E_v$and E_c were defined previously, θ_v is the breadth of the conduction tail. Certainly, Tauc was able to associate the absorption edge with fundamental features in amorphous semiconductors. Cody model is accurate with the interpretation of the energy dependence of the absorption spectrum of *a*-Si:H.

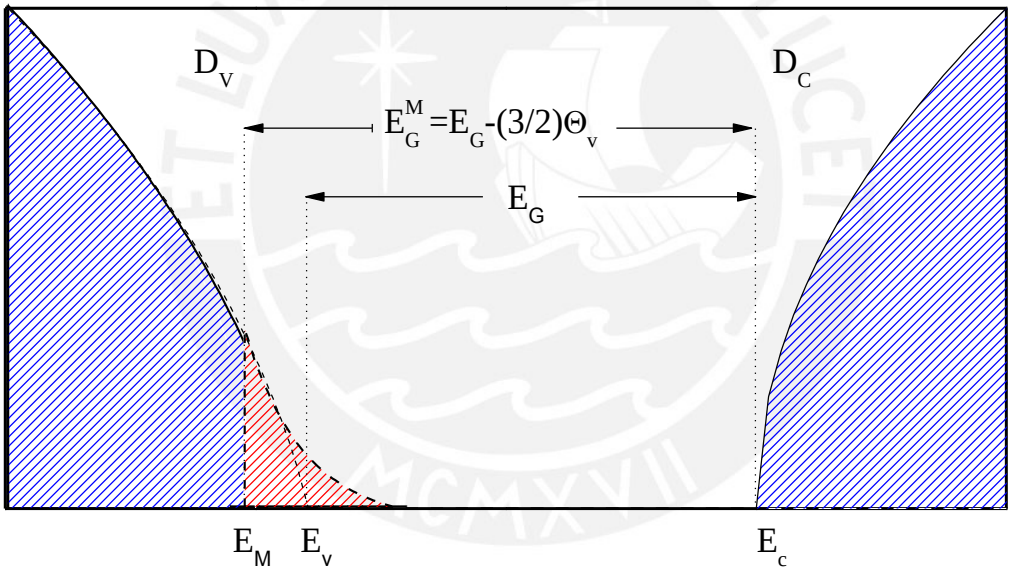

Figure 2.10 The empirical model of density of states considered by **Cody et. al**. [34]

Cody et. al.[34] considered two gaps, the bandgap $E_G = E_c - E_v$ and the mobility gap E_G^M, which depends of the disorder degree.

In 1997 O'leary et. al. [10] presented an elementary empirical model for the distribution of electronic density of states, focusing on the one-electron density-of-states, square-root distributions, and introduce an empirical exponential model for tail absorption region. They consider both regions to be continuous and all transitions to be possible.

$$D_v(E) = C_1 \begin{cases} \sqrt{\frac{\theta_v}{2}} \exp\left(-\frac{1}{2}\right) \exp\left(\frac{E_v - E}{\theta_v}\right), & E > E_v - \frac{\theta_v}{2} \\ \sqrt{E_v - E}, & E \leq E_v - \frac{\theta_v}{2} \end{cases}$$

$$D_c(E) = C_2 \begin{cases} \sqrt{E - E_c}, & E \geq E_c + \frac{\theta_c}{2} \\ \sqrt{\frac{\theta_c}{2}} \exp\left(-\frac{1}{2}\right) \exp\left(\frac{E_c - E}{\theta_c}\right), & E < E_c + \frac{\theta_c}{2} \end{cases}$$

Equation 2.23

Here C_1, C_2 are constants, $E_c + \frac{\theta_c}{2}$ and $E_c - \frac{\theta_c}{2}$ represent the mobility edges of the conduction and valence bands, respectively (see Figure 2.11). Furthermore, in the disorderless limit ($\theta \to 0$) the conduction and valence band function terminate abruptly which corresponds to the case in the absence of disorder.

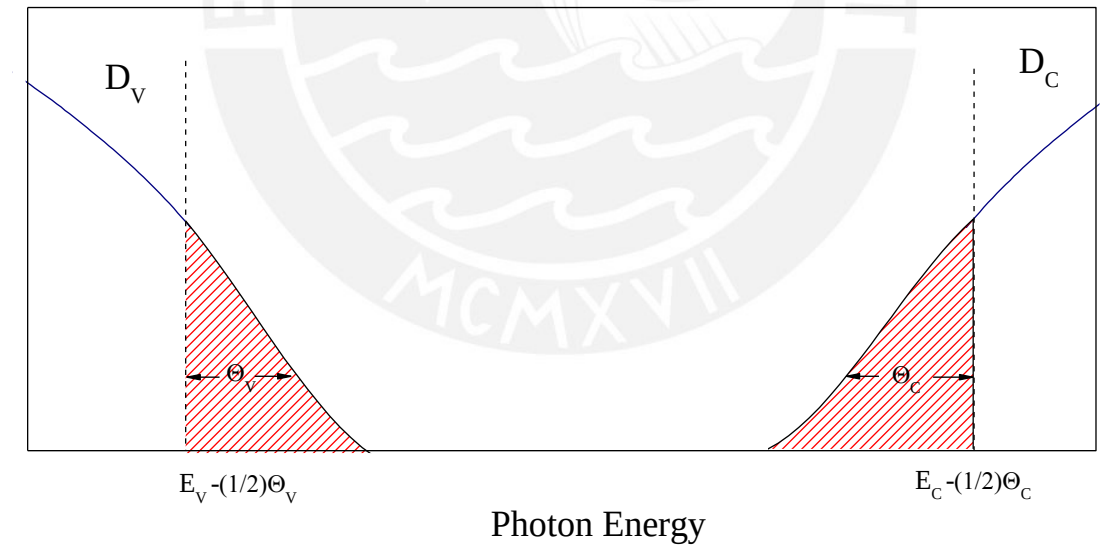

Figure 2.11 The empirical model of density of states considered by O'leary[10]

In 1998 Jiao et. al. [35] considered similar density of states that O'Leary et. al. [10]. The main difference is that Jiao assumed that the exponential tail states intersect the parabolic extended states at the energies E_{vT}, E_{cT}, see Figure 2.12, for the conduction and valence bands, respectively.

$$D_v(E) = C_1 \begin{cases} \sqrt{E_v - E_{vT}} \exp\left(\frac{E_{vT} - E_v}{\theta_v}\right) \exp\left(\frac{E_v - E}{\theta_v}\right), & E > E_{vT} \\ \sqrt{E_v - E}, & E \leq E_{vT} \end{cases}$$

$$D_c(E) = C_2 \begin{cases} \sqrt{E - E_c}, & E \geq E_{cT} \\ \sqrt{E_{cT} - E_c} \exp\left(\frac{E_c - E_{cT}}{\theta_c}\right) \exp\left(\frac{E - E_c}{\theta_c}\right), & E < E_{cT} \end{cases}$$

Equation 2.24

Here C_1, C_2 are constants, E_{vT}, E_{cT} are the intersections between the exponential tail states and the parabolic extended states.

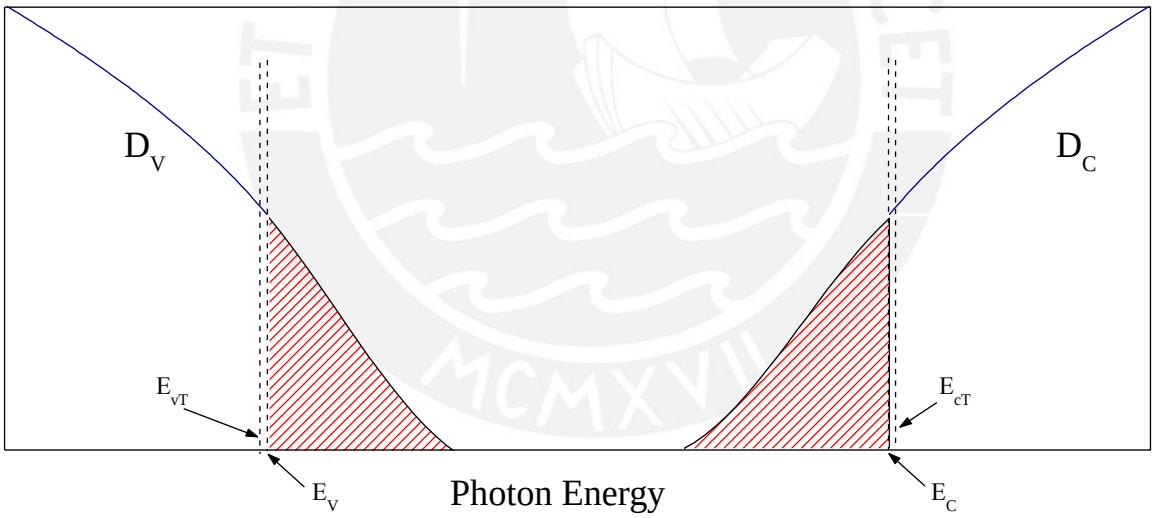

Figure 2.12 The empirical model of density of states considered by Jiao[35]

In 2013 Guerra following the assumption that a disordered material can be studied as an ordered at high temperature (frozen phonon model) proposed a band fluctuations based model [12]. Guerra modeled the topological and thermal disorder by thermal fluctuations in valence and conduction band. Furthermore, Guerra considered the electronic occupation degree in the valence band and the available states in the conduction band by using the Fermi distribution $f(E_c)$, thereby, $D_c \rightarrow D_c(E_c) \times \big(1 - f(E_c)\big)$ and $D_v \rightarrow D_v(E_v) \times f(E_v)$. Following

the Kugo-Greewood formula, Guerra found that the joint density of states (JDOS) can be average by

$$\langle J_{cv}\rangle(E_{cv}) = \int_{-\infty}^{\infty} -f'(E - E_{cv})J_{cv}(E)dE \qquad \textit{Equation 2.25}$$

Here $f'(E - E_{cv})$is the first derivate of the Fermi distribution, $E_{cv} = E_c - E_v$, where $E_c$and E_v representing the conduction band and valence band energies, respectively. In Figure 2.13, DOS and JDOS in this for a fluctuating band is presented. Note that the tail appears in the JDOS.

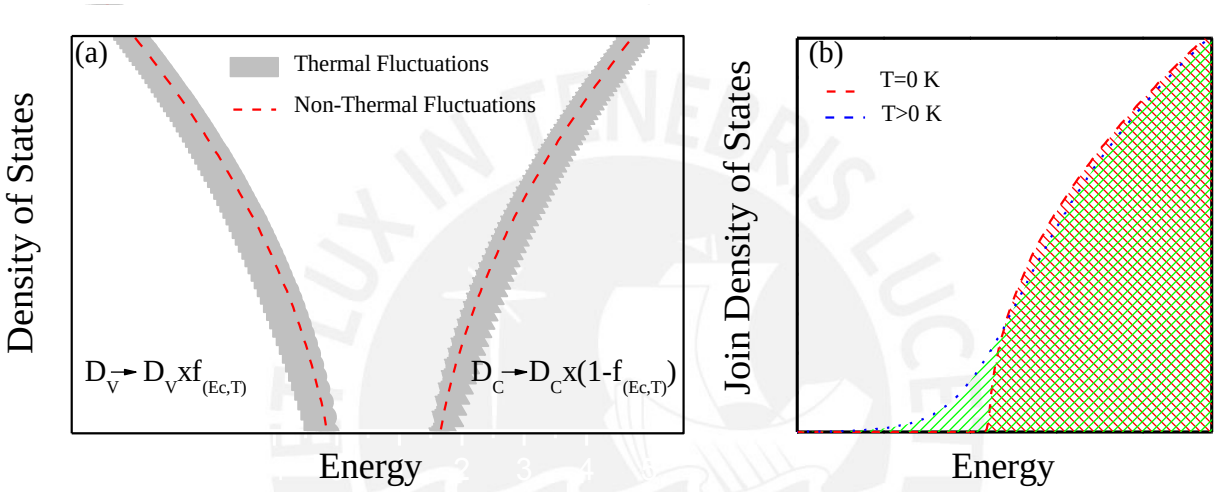

Figure 2.13 The model of density of states considered by J.A. Guerra [12]

2.3.2 The Tauc model

The Tauc model allows quantitative predictions for amorphous silicon according to the experimental data of Cody. Furthermore, it has been widely applied to amorphous semiconductors. Tauc's approach is based in two assumptions. First, that the density of states is parabolic in the valence and conduction bands from the free-electron approximation. Second, the conservation of the wave vector ***k*** is relaxed, **k** is no a good quantum number.

$$\alpha_{Tauc} = \frac{\alpha_0}{\hbar\omega}\iint D_c(E_c)D_v(E_v)\delta(E_c - E_v - \hbar\omega)dE_v dE_c \qquad \textit{Equation 2.26}$$

Solving the integral, in the framework Tauc's model, the absorption coefficient is given by

$$\alpha_{Tauc} = M_{Tauc}^2 \frac{(\hbar\omega - E_{Tauc})^2}{\hbar\omega} \qquad \textit{Equation 2.27}$$

Here $M_{Tauc}^2$is a constant, and according to this model, $\sqrt{\alpha\hbar\omega}$ versus the photon energy is a straight line [36]. The Tauc-gap, E_{Tauc}, is the intercept with energy axes and is considered a measurement of the bandgap in amorphous materials.

2.3.3 The bandgap measurement in amorphous semiconductor

The optical bandgap is one of the most important optical parameters in amorphous semiconductors. different methods to determinate the bandgap in amorphous can found [37] [38]. However, for many years the Tauc model has served as the standard empirical model whereby the optical gap of an amorphous semiconductors may be determined.

$$\sqrt{\alpha_{(\hbar\omega)}\hbar\omega} = M_T(\hbar\omega - E_{Tauc}) \qquad \textit{Equation 2.28}$$

Tauc concluded that an extrapolation of the essentially linear functional dependence of Equation 2.28, at sufficiently large in Energy, allowed an empirical bandgap. Furthermore, the isoabsorption method called E_{04}[39], [40], it is also widely applied.

2.3.4 The Urbach model

In 1953, Urbach showed experimentally that exponential tail absorption increase with the incident photon [6]. Then, a larger number of amorphous semiconductors study the tail absorption by Urbach model [7].Which is a universal feature of the absorption edge of amorphous semiconductors and insulators. The nature of disordering can be intrinsic due structural defects (vacancies, interstitial or dislocation) and by temperature effect. The dependence of absorption coefficient, at the Urbach edge, on the photon energy is typically given by

$$\alpha(E) = \alpha_F \exp\left(\frac{E - E_F}{E_u(X,T)}\right) \qquad \textit{Equation 2.29}$$

Here α_F, E_F are constants related to the Urbach focus, as will be discussed later, $E_u(X,T)$ is an indirect measure of the disorder degree. Then, the Urbach energy,E_u, reveals the influence from static (‘frozen’ phonon) and dynamic (thermal phonon) disordering via displacement of atoms from their equilibrium position[41]. the Urbach energy can be written

$$E_u(T,X) = K\{\langle u^2\rangle_T + \langle u^2\rangle_x\}$$ *Equation 2.30*

Where K is a constant, $\langle u^2\rangle_T$, $\langle u^2\rangle_x$ are is the mean square displacement of the atoms due to the thermal and structural disorder, respectively, both contributions are independent, additive and, in adiabatic approximation, have a similar effects on the electronic levels [42]. Additionally, the displacement of the atoms due to the thermal vibrations and structural generate in the absorption edge to the electron-phonon interaction. The Equation 2.31 can be rewritten as electric potential of the system:

$$E_u(T,X) = K_w\{\langle W^2\rangle_T + \langle W^2\rangle_x\} = (E_u)_T + (E_u)_x$$ *Equation 2.31*

Where K_w is a constant, $\langle W^2\rangle_T$ is a mean-square deviation from the electric potential related disordering due to the temperature in a ideally ordered structure, $\langle W^2\rangle_T$ is due to structural disorder [43]. Now, amorphous materials present parallel shift of the absorption edge in the temperature range, in consequently $\langle W^2\rangle_x$ present to components static and dynamic disordering [44]. Moreover, the Equation 2.31 can be rewritten

$$E_u(T,X) = (E_u)_T + (E_u)_{x,sta} + (E_u)_{x,dyn}$$ *Equation 2.32*

Here $(E_u)_{x,sta}$, $(E_u)_{x,dyn}$ are the static and dynamic disordering contribution, respectively. The contribution by $(E_u)_{x,sta}$ represent the absence of the long-range order in the solid and $(E_u)_{x,dyn}$ is the contribution by absence of the intermediary-order. Thus, it has been reported that at high temperature of As_2S_3 (~300K) is gradually established the intermediate order that resulting in the decrease of $(E_u)_{x,dyn}$[43]. However, the contribution by $(E_u)_{x,sta}$ is constant. The study of $(E_u)_T$, $(E_u)_{x,sta}$and $(E_u)_{x,dyn}$ are through the Einstein model [43]. The Equation 2.30 can be expressed as

$$E_u = (E_u)_0 + (E_u)_1\left[\frac{1}{\exp\left[\frac{\theta_E}{T}\right]-1}\right]$$ *Equation 2.33*

Here $(E_u)_0$and $(E_u)_1$ are a constants, $\theta_E$the Einstein temperature.

2.3.5 Generalization of the fundamental absorption in amorphous semiconductors.

The aim is to develop an understanding of the optical response of amorphous semiconductors over the spectral range corresponding to the Urbach and Tauc regions. To do so, the theoretical basis for the interpretation of the optical absorption spectrum is provided. Following the analysis performed by Guerra et. al. [12] in which the topological disorder is introduced by thermal band fluctuations. Optical absorption spectrum within the framework of this model is studied. To begin, the electronic transition rate between the extended valence and conduction bands, Equation 2.8.

O'Leary evidenced by electron and hole drift mobility measurements the potential fluctuations between the conduction and valence bands[10][45]. O'Leary proposed treating the JDOS as a local JDOS over the distribution of conduction and balance bands.

$$\langle J_{(\hbar\omega)}\rangle = < \int D_c^{Loc}(E) D_v^{Loc}(E-\hbar\omega) dE > \qquad \textit{Equation 2.34}$$

$D_{c/v}^{Loc}(E)$ is the local conduction and valence band DOS. O'Leary demonstrated that Equation 2.34 can be considered as a generalization of the traditional approach of Tauc. The average of the JDOS can be expressed by:

$$\langle J_{cv}\rangle = \int J_{cv}(E)\widehat{W}_{(E-E_{cv})} dE \qquad \textit{Equation 2.35}$$

$\widehat{W}$ is the weight function, $E_{cv} = E_c - E_v$, where $E_c$and E_v representing the conduction band and valence band energies, respectively. The average JDOS in the Fermi's golden rule can be introduce and relax the momentum conservation.

$$\langle R_{cv}\rangle = \frac{2\pi}{\hbar}\left(\frac{\tilde{E}e}{2\omega m_e}\right)^2 \int |M_{cv}|^2 J_{cv}(E_{cv})\widehat{W}_{(E_{cv}-E)} dE_{cv} \qquad \textit{Equation 2.36}$$

$|M_{cv}|^2$ is the matrix element of the optical transitions, who dependence with the energy is negligible and $\langle R_{cv}\rangle \sim \langle J_{cv}\rangle$ depends directly of the weight function. Note that by using $\widehat{W} \longrightarrow \delta(E_{cv}-\hbar\omega)$ it is recovered the traditional Tauc calculation. O'Leary introduced a Gaussian distribution as weight function while Guerra used the derivative of the Fermi distribution [33][12]

$$\widehat{W} \longrightarrow -\frac{df(E)}{dE}$$

Here $f(E)$ denotes the Fermi distribution. On the other hand, Guerra presented used this weight function motivated in the Kugo-Greewood formula the absorption coefficient can be written as follows shown in equation 2.35 and 2.36. More details can be found in[46][12]

$$\alpha(\hbar\omega, T) = \frac{\alpha_0}{\hbar\omega}\int \int D_c(E_c)D_v(E_v)(-1) \times f'(E_c - E_v - \hbar\omega)\ dE_v dE_c \qquad \textit{Equation 2.37}$$

Where α_0 absorbs the constants including the transition matrix element. By integrating Equation 2.37 the functional form of the optical absorption spectrum can be determined.

$$\alpha(\hbar\omega) = -\frac{\pi}{4}\frac{\alpha_0}{\beta^2\hbar\omega}\mathrm{Li}_2\left(-e^{\beta(\hbar\omega - E_0)}\right) \qquad \textit{Equation 2.38}$$

Here β is defined as $\beta = 1/(k_B T)$. And is equivalent to the Urbach slope. E_0 is defined as the energy difference between the mobility edges. $E_0 = E_c(0) - E_v(0)$. $\mathrm{Li}_2(x)$ is the di-logarithm function of *x*. Figure 2.14 depicts the absorption coefficient of *a*-Si:H along with a fit using equation 2.38. The model captures the distributions of tail states and band-to-band transitions. Furthermore, the optical absorption coefficient blends into both regions. It is pointed out that traditional means due which the region between Urbach and Tauc through the fitting could be used. Now, an asymptotic analysis of Equation 2.38 leads to similar expressions obtained by Urbach and Tauc, Guerra called extended Urbach and extended Tauc these equations, respectively (see Equation 2.39). Note that at cero Kelvin (or 0 meV Urbach energy) the extended Tauc expression is reduced to the traditional Tauc model.

$$\alpha(\hbar\omega) = \frac{\pi}{8}\frac{\alpha_0}{\hbar\omega}\begin{cases} \frac{2}{\beta^2}e^{\beta(\hbar\omega - E_0)} & , \quad \hbar\omega \ll E_0 \\ (\hbar\omega - E_0)^2 + \frac{\pi}{\beta^2} & , \quad \hbar\omega \gg E_0 \end{cases} \qquad \textit{Equation 2.39}$$

Figure 2.14 also depicts the asymptotical curves. Our results show that the extended Urbach and Tauc equations are within of the Urbach and Tauc region, respectively.

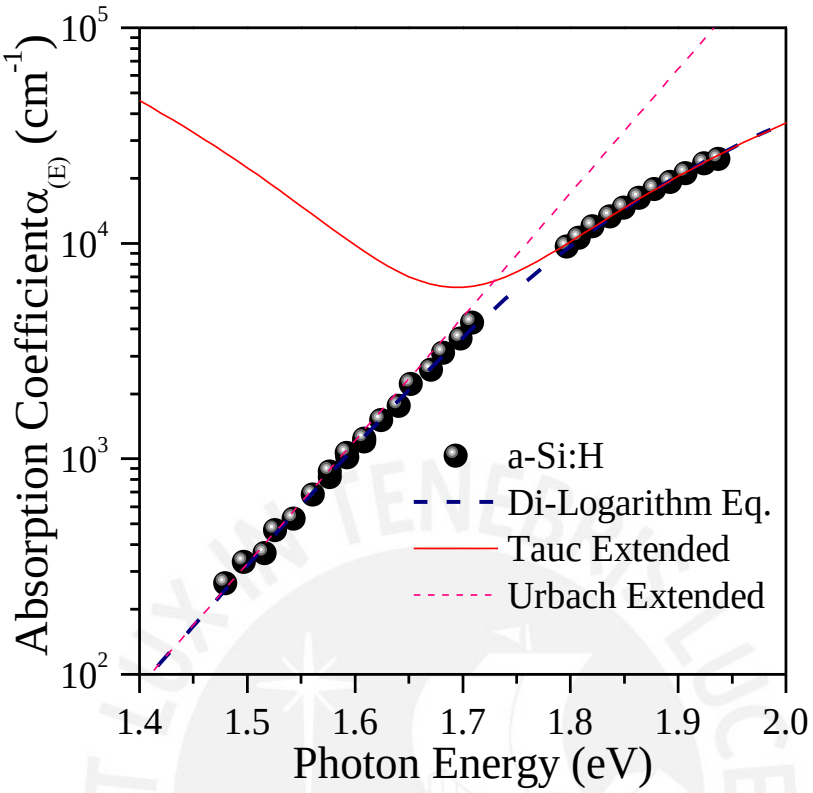

Figure 2.14 The optical absorption spectrum, $\alpha_{(E)}$ versus the photon energy, associated with a-Si:H. The experimental data of Cody et. al.[47]*. The points correspond to experimental data. The solid line is the equation indicated in the legend within Figure.*

The bandgap in absence of disorder, E_0, which is a measurement of the mobility edge between the valance band and conduction band. E_0 can be modified by the chemistry and structure of the material. For instance a reduction of the lattice parameter, $\langle r_i{}^2 \rangle$, will be translated in an increase of E_0. Furthermore, the Tauc-gap is sensitive to both the mobility band edges and Urbach tails. In this sense, the proposed model allows us the measurement of a parameter independent of the disorder degree, the advantage that is no necessary to discriminate the Urbach and Tauc regions beforehand.

2.4 Urbach focus

The Urbach focus concept has been employed extensively for a-Si:H [48], [49] and other amorphous materials [12], [50]. However, the real physical meaning has been extensively discussed and different approaches were taken to estimate the Urbach focus[12], [50], [51]. The exponential tail observed in amorphous semiconductors is usually described by the Urbach

model (equation 2.40). The structural disorder can be manipulated by thermal annealing treatments for instants and is reflected on the width of the exponential tail. The Urbach focus is the apparent constant point appearing in a material when measuring the absorption coefficient under different disorder degrees. This focus can be calculated as the extrapolation of the Urbach tails towards higher energies in logarithm scale as shown in figure 2.15.

$$\alpha(E) = \alpha_F \exp(\beta(E - E_F))$$ *Equation 2.40*

Here $\beta = 1/E_U$ is the Urbach slope, α_F is the pre-exponential constant and E_F is characteristic energy independent of the amount of disorder. The coordinate $(\alpha_F; E_F)$ is the Urbach focus.

The Urbach focus is considered a parameter independent of the amount of disorder and therefore an intrinsic property of materials. However, the meaning of the value is extensively discussed. Different authors proposed several models. In this sense, in the next section three estimation approaches and propose a new analysis taking advantage of the extended Urbach rule is introduced.

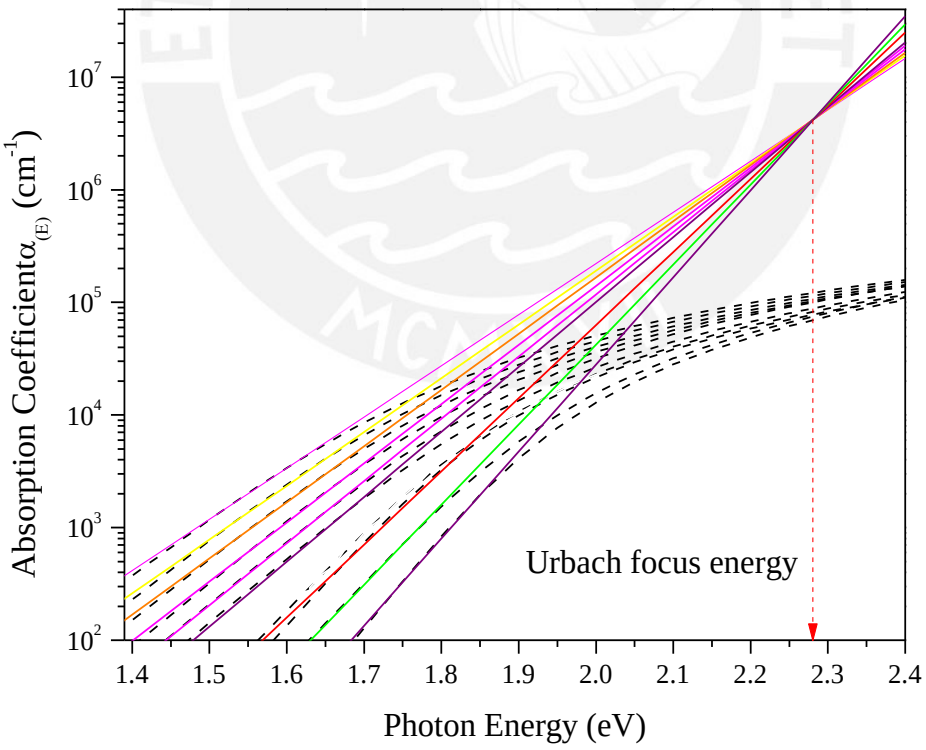

Figure 2.15 Schematic representation of Urbach focus. Dotted lines is the absorption coefficient representation with different width of the exponential tails and Solid line is the Urbach model.

2.4.1 Global fit

In order to find the Urbach focus, typically, one writes the χ^2_{all} estimator as summation of χ^2_i corresponding to each tail. The parameters α_F and E_F are shared (are the same) for all these individual estimators, see Equation 2.41, where N is the number of fitting curves. Thenceforth the estimator χ^2_{all} is minimized. Figure 2.15 shows the Global fit method. However, this method could be consider as an artifact mathematical of the particular of the fitting process.

$$\chi^2_{all}(\beta_1, \beta_2 \ldots, \beta_N, \alpha_F, E_F) = \sum_{i=1}^{N} \chi^2_i(\beta_i, \alpha_F, E_F) \qquad \textit{Equation 2.41}$$

2.4.2 Cody's relation

Cody, in the framework of the study the disorder effect in *a*-Si:H [4][48] introduced the temperature and thermal annealing effects and found a relation between the Urbach energy and bandgap in amorphous materials. Following the Urbach model and according to Cody the bandgap in semiconductors is written as

$$E_g(T, X) = E_g(0,0) - D\{\langle u^2\rangle_T + \langle u^2\rangle_x - \langle u^2\rangle_0\} \qquad \textit{Equation 2.42}$$

Here $E_g(0,0)$ represents the bandgap in absence of disorder, $\langle u^2\rangle_0$ is the mean square atomic displacement in the absence of disorder. $\langle u^2\rangle_T$ and $\langle u^2\rangle_x$ are is the mean square displacement of the atoms due to the thermal and structural disorder, respectively. The latter contributions are independent and additive. Furthermore, from the Urbach definition and consider the Equation 2.42 the bandgap as a function of the Urbach energy can be write [48]:

$$E_g(T, X) = E_F + GE_u(T, X) \qquad \textit{Equation 2.43}$$

Here $E_g(T, X)$ is the bandgap, E_F is Urbach focus, G is a constant and E_u is the Urbach energy. Afterwards, Cody defined the Urbach focus by, $E_F = E_g(X = 0, T = 0)$ for $E_U(X = 0, T = 0) = 0$ [31]. It is important to mention that the bandgap presents different approximations. These were introduced in section 2.3.3. According to different authors the Tauc band gap is applied to evaluate the lineal relation, between Tauc gap and Urbach energy values, in semiconductors materials as a-Si: H, a-SiC and a-SiC:H [48] [46].

2.4.3 Orapunt and O'Leary's approach

According to Orapunt and Oleary, it is possible to calculate the Urbach focus without a bias [49].They expressed the Urbach model (Equation 2.29) as

$$\alpha(E) = \alpha_0 \exp\left(\frac{E}{E_u}\right) \qquad \textit{Equation 2.44}$$

and

$$\alpha_0 = \alpha_F \exp\left(-\frac{E_F}{E_u}\right) \qquad \textit{Equation 2.45}$$

Where α_0 is the pre-exponential in the Urbach rule, E_u is the Urbach energy. Now, if Equation 2.44 in logarithmic scale is expressed and β is considered as $= 1/\,E_u$, a linear function which is represent as

$$Ln[\alpha(E)] = \boldsymbol{Ln}[\boldsymbol{\alpha_0}] + \boldsymbol{\beta} E \qquad \textit{Equation 2.46}$$

From the fitting process, in logarithm scale, by least-square for each spectra of the optical absorption independently in the Urbach region and the set of parameters ($\boldsymbol{\beta}, \boldsymbol{Ln}[\boldsymbol{\alpha_0}]$) is obtained, which can be represented as in Equation 2.47 and it is represent by Ω as the pre-exponential in the Urbach rule, $\Omega = Ln[\alpha_0]$.

$$\Omega = \boldsymbol{Ln}[\boldsymbol{\alpha_F}] + \boldsymbol{E_F}\beta \qquad \textit{Equation 2.47}$$

The linear function Ω, allow to find the Urbach focus by the slope and intercept. In several semiconductors materials will be evaluated. Additionally, it is important to mention that this method use independent fits which in contrast to the global fit does not introduced a numerical bias.

2.4.4 Our approach

The extended Urbach rule is used, Equation 2.39, which was obtained by asymptotic analysis of the dilogarithm equation. Using the setting of parameters found in the dilogarithm equation (α_0, β, E_0) and contrasting them with the traditional Urbach rule. To begin, the Urbach focus is actually a region and that both equations are nearly, see Figure 2.16.

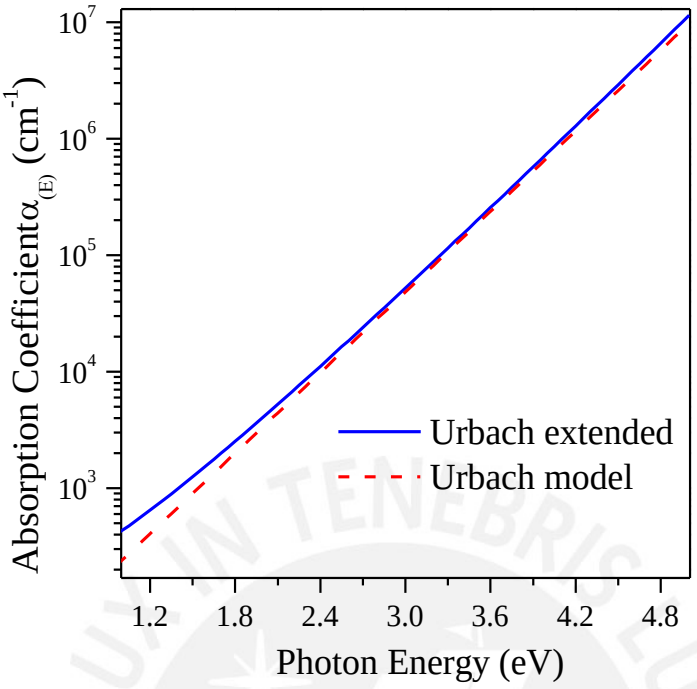

Figure 2.16 Urbach rule and extended Urbach rule plotted together with similar parameters for comparison reasons only.

Therefore, both equations around the Urbach focus can be written as

$$\alpha_{(E)}^{U'} = \alpha_{(E)}^{U}, E \sim E_F \qquad \textit{Equation 2.48}$$

Where $\alpha_{(E)}^{U'}$ is the extended Urbach rule and $\alpha_{(E)}^{U}$ is the Urbach rule. In the same way, both equations in Urbach focus value are evaluated

$$\frac{\pi}{4}\frac{\alpha_0}{E_F\beta^2}e^{\beta(E_F-E_0)} = \alpha_F e^{\beta_u(E_F-E_F)} \qquad \textit{Equation 2.49}$$

The terms are rearranged and written in Equation 2.49 . Then, a linear relationship is represented as

$$\ln\left[\frac{\pi}{4}\frac{\alpha_0}{\beta^2}\right] - \beta E_0 = -\beta E_F + \ln[\alpha_F E_F] \qquad \textit{Equation 2.50}$$

Finally, the term Ψ is defined, and it is showed the linear relationship as

$$\Psi = -\beta E_F + \ln[\alpha_F E_F] \qquad \textit{Equation 2.51}$$

$\alpha_{F,}E_F$ represent the Urbach focus. Finally, the plot β versus Ψ are fitted, then, the slope represent the Urbach focus energy.

3. Results and discussion

This section, the sensitivity of the Guerra's model is evaluated by introducing changes disorder degree and how it is affected in Tauc gap and mobility gap. Afterwards, in section 3.2 the optical characterization of hydrogenate amorphous silicon is studied. In order to validate the model this is applied not only to *a*-Si:H, furthermore, to *a*-SiC:H and *a*-SiN. Finally, the implications of the Urbach focus concept due that represents a parameter independent of disorder degree is explored and it is still widely discussed. However, several analysis is introduced.

3.1 The sensitivity of the Guerra's model

The aim is to develop an understanding of the optical response of amorphous semiconductors over the entire spectral range, Urbach and Tauc regions. In the present section, the sensitivity of the Di-logarithm function, Equation 2.38, is examined upon the modification of the band-tails breadth ($E_u = 1/\beta$), all other parameters being held fixed at their nominal hydrogenated amorphous silicon values. the independence between E_0 from to E_T , E_u is presented.

In Figure 3.1, the setting of parameters (α_0, β, E_0) is determined from the fits performed to the experimental *a*-Si:H optical absorption data sets of Cody et al. [42] at different temperatures. However, the curves are generated with α_0, E_0 fixed at 1.69 $\times 10^6 cm^{-1}$ and 1.76 eV, respectively.

In order to assess the impact of the Urbach energy, within the framework of the simple model of Guerra[1][12]. The Tauc-gap determined by using the relationship for amorphous solids ($\sqrt{\alpha E} = M_T(\hbar\omega - E_T)$, where $\hbar\omega$ is photon energy[5]), and Urbach energy (E_u), found by using the exponential behavior at band-edges in logarithm scale ($Ln[\alpha(E)] = \boldsymbol{Ln[\alpha_0]} + \boldsymbol{\beta} E$), are evaluated and plotted as a function of $\hbar\omega$ in Figure 3.1a and b, respectively. In Figure 3.1a, a local point is showed, called Urbach focus, where in section 3.5 will be discussed, however, here it is showed as a consequence of the fit in the Urbach region.

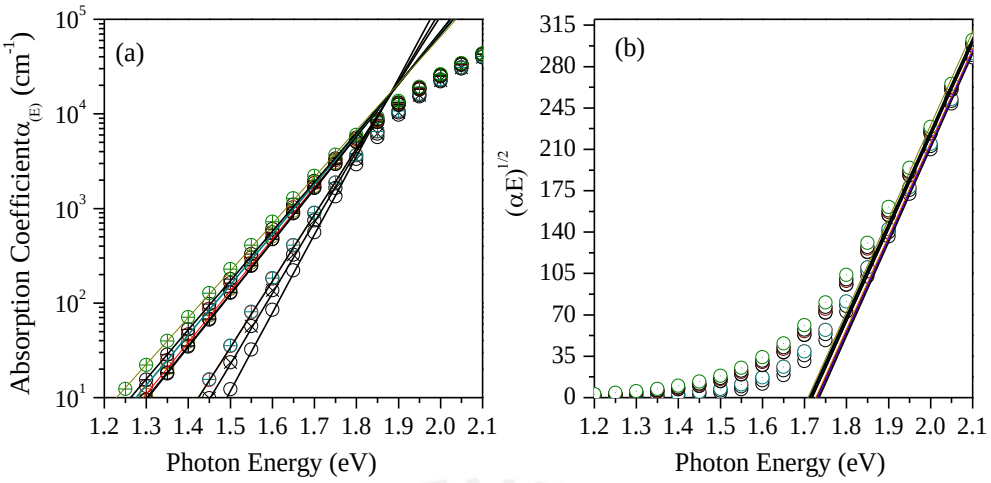

Figure 3.1 Absorption coefficient generated with the equation Equation 2.38 evaluated on different Urbach energy values, and with α_0, E_0 fixed. (a) Urbach region is fitted in logarithm scale, (b) Tauc plot

Figure 3.2 b E_u is varied from 58.23 meV to 80.42 meV, and in agreement with our prediction, the linear relation with Tauc energy is shown, following the classical models. Figure 3.2 b. the parameter $E_0$is independent of the disorder degree. This is the first analysis to understand the behavior of dilogarithm function and extract information of the Guerra's model. In the next section, the characterization of amorphous semiconductors materials is presented.

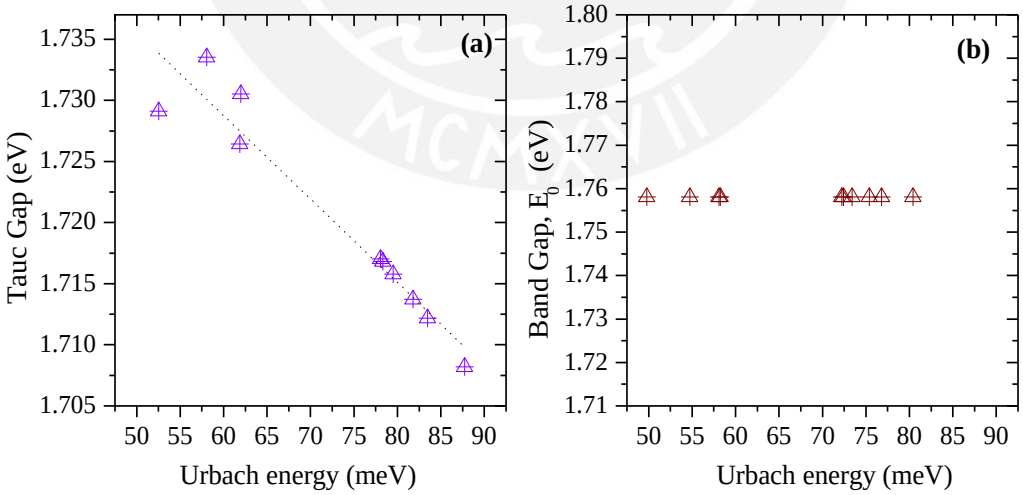

Figure 3.2 (a) Linear relation of Tauc and Urbach energy. (b) Here E_0 is an independent parameter of disorder degree, Urbach energy

3.2 Optical characterization of hydrogenated amorphous silicon

The presented model with hydrogenated amorphous silicon (*a*-Si:H) is tested first since it is one of the most important electronic materials. To begin, the data obtained in this study was fitted by J. A. Guerra's model in the entire absorption coefficient spectra, Equation 2.38, and the classical models: (i) Urbach model, in the absorption exponential and (ii) Tauc model, characterizing the transitions between extended states or band-to-band transitions. First, the fitting process with Guerra's model has been applied on the logarithm scale, which is a manner of visualizing data that are associated with exponential and fundamental absorption region, thereby, a better performance of the Guerra's model fit can be do and the error can be diminished by the fitting process in logarithm scale. Then, non-linear regression is performed on the data with the Guerra's model, which was worked in the Mathematica software environment. In this regards, from least squared fit, three parameters for each spectrum is founded: (i) the Urbach energy $E_u = 1/\beta$, (ii) the bandgap in absence of disorder degree E_0 and one parameter which is related to (iii) electronic transition matrix element between the conduction and valence band α_0. The fits are depicted in Figure 3.3. the Guerra's model is suitable to describe the optical behavior of *a*-Si:H.

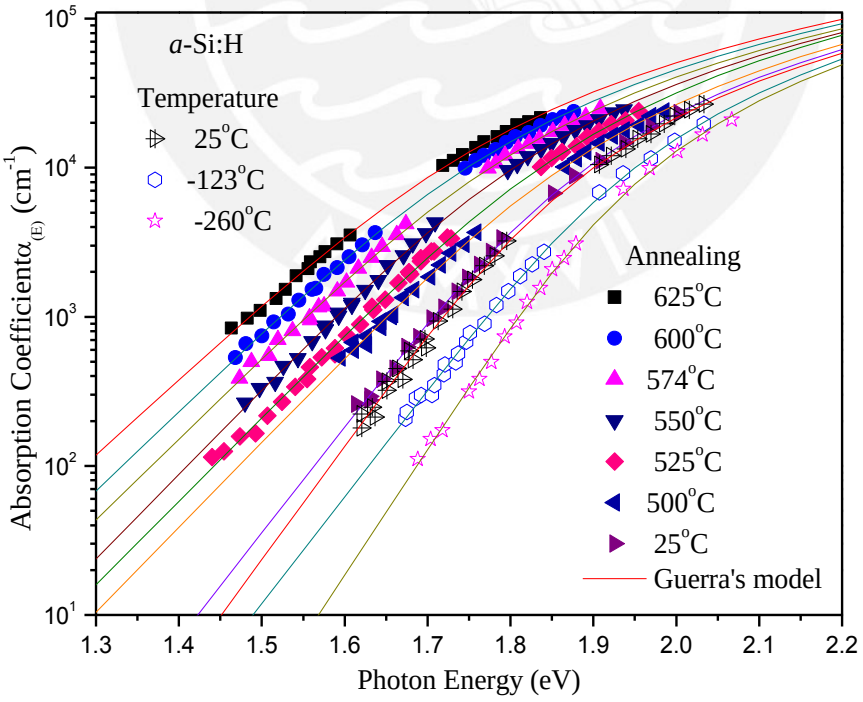

Figure 3.3 The optical absorption spectrum,$\alpha_{(E)}$ versus photon energy, associated with a-Si:H. The experimental data of Cody et. al.[47]. *The color scheme is indicated in the legend within Figure.*

The optical bandgap of amorphous semiconductors is a rather debatable parameter since in an amorphous semiconductor, the tail states in the absorption coefficient presents into the gap region, in contrast, in a crystalline semiconductor, the optical absorption coefficient terminates abruptly at the energy gap. In this sense, the Tauc equation is widely used to define the bandgap in amorphous semiconductors [52] and is comparable with iso-absorption bandgap E_{04} [29][30] and Sokolov gap [37]. The Tauc-analysis, from the fundamental absorption region, suggests an extrapolation of the apparent linear function dependence, this is plot $\sqrt{\alpha E}$ versus the photon energy, see Figure 3.4 (a), the intercept with the axis of energy give us the value E_t.

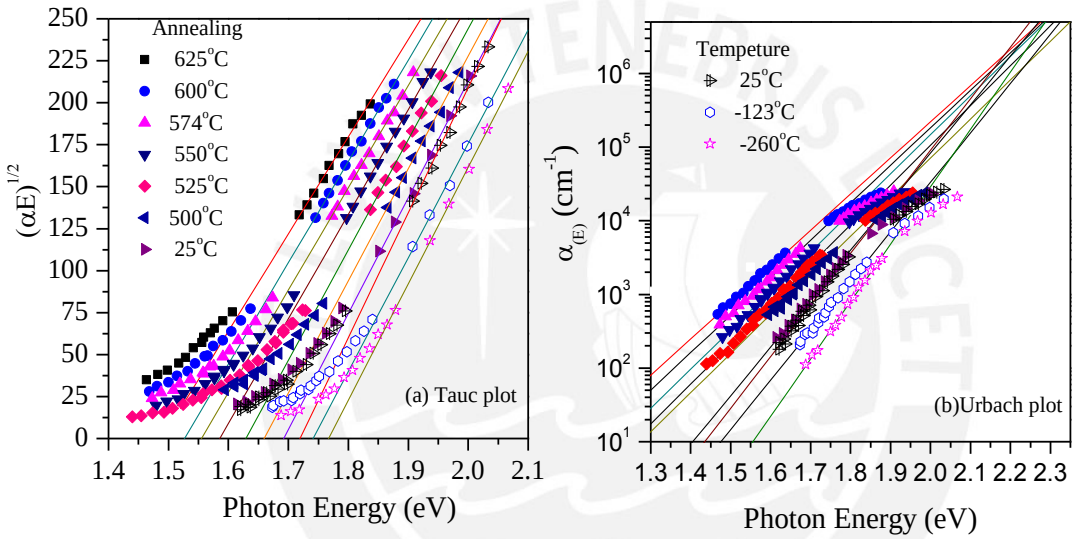

Figure 3.4 (a)The Tauc gap. the Tauc extrapolations corresponding to the hydrogenated amorphous silicon data is showed [47]. *The data are depicted with the solid and open points, the least-squares fits to Tauc model being indicated with the solid lines. (b)* The breadth of the optical absorption tail E_u

The Urbach model in the exponential region was applied. Though of the semi-log plots of the absorption coefficient versus photon energy shows an extended linear region, a value for the Urbach energy is often given by the slope β, see Figure 3.4 (b). the results show important changes of the different parameters determined after annealing. Table 3.1 summarizes the results obtained from the fitting process. It's important to mention that the bandgap in the absence of disorder and Urbach energy can be calculated simultaneously with a simple fit only. In contrast with the traditional model that has been required bisect the optical absorption in two regions.

Table 3.1 The best fitted parameters corresponding to the fits to the experimental a-Si:H optical absorption data sets of Cody et al. [47] *are shown in Figure 3.3*

Temperature (°C)	Classical model		Guerra's model	
	Urbach energy (meV)	Tauc gap (eV)	Urbach energy (meV)	Band gap 'E_0' (eV)
T_M=-260.8	55.73	1.77	49.79	1.84
T_M=-122.5	64.72	1.74	58.1	1.83
T_M=19.5	62.01	1.72	54.74	1.75
25.5	65.92	1.69	58.23	1.76
T_H=499.5	81.83	1.66	72.22	1.75
T_H=524.5	80.29	1.63	73.43	1.74
T_H=549.5	81.8	1.59	72.43	1.69
T_H=574.5	85.37	1.56	75.38	1.66
T_H=599.5	88.32	1.53	76.81	1.64
T_H=624.5	94.09	1.49	80.42	1.61

3.2.1 The bandgap and Urbach energy of *a*-Si:H

The *a*-Si:H material presents a random covalent network of Si-Si and Si-H bonds, the hydrogen in the *a*-Si:H network plays an important role due the fact that the presence of hydrogen atoms reduces the dangling bonds density which reduces the disordered structure [53] [54]. *a*-Si and *a*-Si:H are metastable materials, which present excess energy and unstable with respect to the crystalline case. This excess energy in materials stems from the energy input received during the growth film[55].

The three first points, in Figure 3.5(a), correspond to temperature changes in the sample. The E_0 is a direct measure of the energy gap between the mobility edges and is independent of the Urbach tails. The bandgap variation as a function of temperature, $T\ vs\ E_0$, which is usually used to calculate nonlinear temperature dependent bandgap change as established by Varshni equation [56]. Therefore, E_0 is dependent on the temperature changes in the sample, Figure 3.5 (a). On the other hand, the Tauc-gap is sensitive to both: the mobility edges and the Urbach energy as shown earlier, section 3.1, and, therefore, applying the Varshni equation to the Tauc-gap versus the temperature would be misleading [56]. Then, the variation with the temperature observed in E_0 is a direct measure of the effect of the temperature on the lattice constant and therefore on the

bandgap of the material. It is found that the Urbach energy is not correlated to E_0. Notice that with the Guerra's model the two values of E_0 obtained at room temperature match pretty well.

The variation of the Tauc-gap with the annealing temperature is illustrated in Figure 3.5(a). The general shape of all the curves agrees very well with others works[47][33]. It is known that the optical bandgap increases with the hydrogen incorporation. This is due to dangling bonds decrease[57]. The effect of the annealing temperature in the fundamental absorption of *a*-Si:H was reported by Y. Laaziz [57]. Laaziz showed that the hydrogen concentration in *a*-Si:H thin films decrease with the annealing temperature between 300 and 500 ºC. This effect has been reported in materials like *a*-SiC:H [58], [1]. The thermally-induced hydrogen loss altered the structure as the dangling bonds density increased and the stress in the lattice was increased [53]. The Tauc-gap, sensitive to the disorder modification, decreased after 500 ºC annealing temperature. This diminution is progressive for all annealing temperatures, see Figure 3.5 (a). The E_0 bandgap exhibits a similar behavior than the Tauc-gap in the annealing region and suggests a diminution of the energy separation between the mobility edges or increment of the average of lattice parameters.

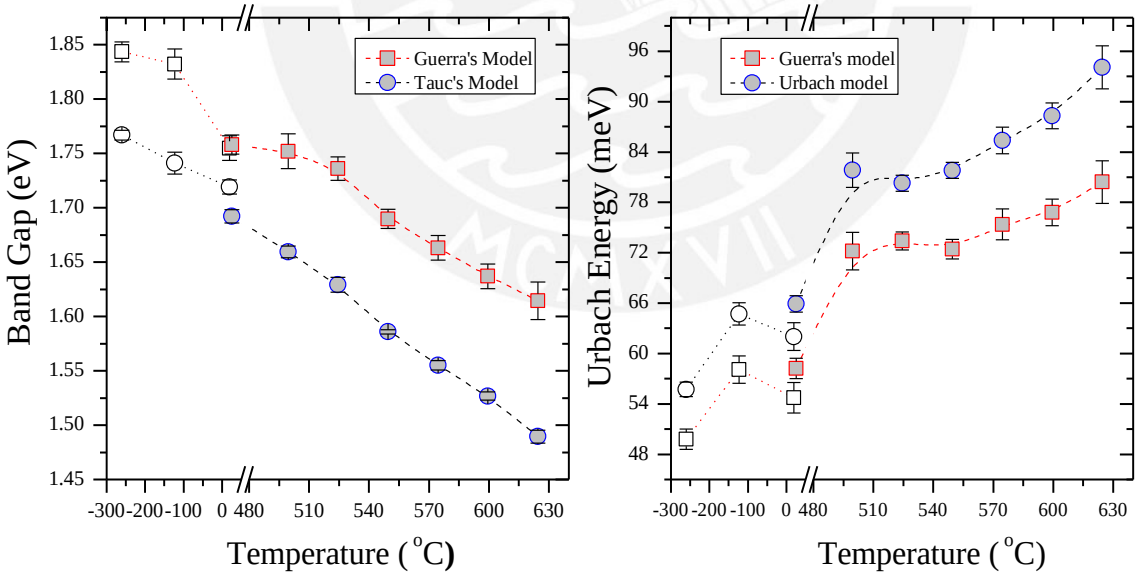

Figure 3.5 Optical bandgap (a) and Urbach energy (b) versus the temperature. Open symbols correspond to sample under measured under different temperatures. Filled symbols correspond to the sample annealed at the shown temperatures.

The Urbach energy gives us the measure of the width of the tail states which contain both the effect of the static and thermal disorder. Indeed, defects play an important role in shaping the spectrum of optical absorption coefficient [59]. In hydrogenated amorphous silicon case, J. J. Thevaril demonstrated that the conduction band-tail breadth is always smaller than the valence band-tail breadth [60]. Cody induced structural disorder intentionally in the films by introducing dangling bonds through the thermal evolution of hydrogen out-diffusion. In this sense, the Urbach energy is correlated with the sharpness of the band tail and hence provides information about defect density as dangling bonds[32].

Figure 3.5 (b), depicts the variation of the Urbach energy with the annealing temperature and for 3 different samples temperatures. The first three points correspond to temperature variation which relates to thermal effect on the Urbach energy. Both models, the Urbach and Guerra's models present a similar behavior with temperature. The relationship between the defect density and annealing temperature was studied by M. Stutzmann [32]. Stutzmann shows that the Urbach energy reflects into the dangling bond density for an increase of E_u. Nonetheless, E_u increase with the annealing temperature.

The key result of the presented analysis is the correlation between the Tauc-gap and Urbach energy. When the Urbach energy increases the Tauc-gap decreases. To sum up, our measurement of the bandgap exhibited a similar behavior with Tauc-gap, because the chemistry changed as soon as the hydrogen concentration decreased, thereby, E_0 decreased. The bandgap E_0 suggests a diminution of the energy separation between the mobility edges or increment of the average of lattice parameters. On the other hand, the Urbach energy increased due the stress in the lattice by the hydrogen loss and defects appear into.

3.3 Optical characterization of hydrogenated and non-hydrogenated amorphous silicon carbide

In the framework of the research realized in the Solid State Physics group at the PUCP *a*-SiC:H layers were produced on polished crystalline calcium fluoride (CaF_2) substrates by RF magnetron sputtering in a 5N purity argon-hydrogen atmosphere mixture using a high purity crystalline SiC target with a diameter of 51 mm. Table 3.2 enlists the different deposition parameters used for growing the films. Three different hydrogen fluxes were used during the

deposition process, the samples were subjected to post-deposition isochronal thermal annealing treatments in a quartz tube with a constant argon flux at 2.6 x 10^{-2} mbar. The annealing temperature ranged from 300 ^{o}C to 700 ^{o}C in steps of 100 ^{o}C for 15 min each. More details concerning the deposition, annealing and characterization conditions can be found in [46][1].

Table 3.2 Deposition conditions of the SiC layers grown with 0 sccm (i), 5 sccm (ii) and 15 sccm (iii) hydrogen flux[1].

Material	Ar (sccm)	H_2 (sccm)	Power (W)	Time (min)	Pressure (mBar)
(i)*a*-SiC	50	0	120	143	1.5 10^{-2}
(ii)*a*-SiC:H_x	50	5	120	270	9.0 10^{-3}
(iii)*a*-SiC:H_x	35	15	120	330	1.2 10^{-3}

The absorption coefficient spectra presented in this thesis are all obtained from optical transmission, in the range from 190 nm to 1100 nm (UV-VIS). The optical constants of *a*-SiC:H_x were determined in the photon energy range 1.15-5 eV, with the aim to obtain information about electronic structure. Following the procedure in *a*-Si:H case, the Guerra's model, Equation 2.38 to fit by the least squared method the absorption coefficient. Three parameters for each spectrum (α_0, β, E_0) was found.

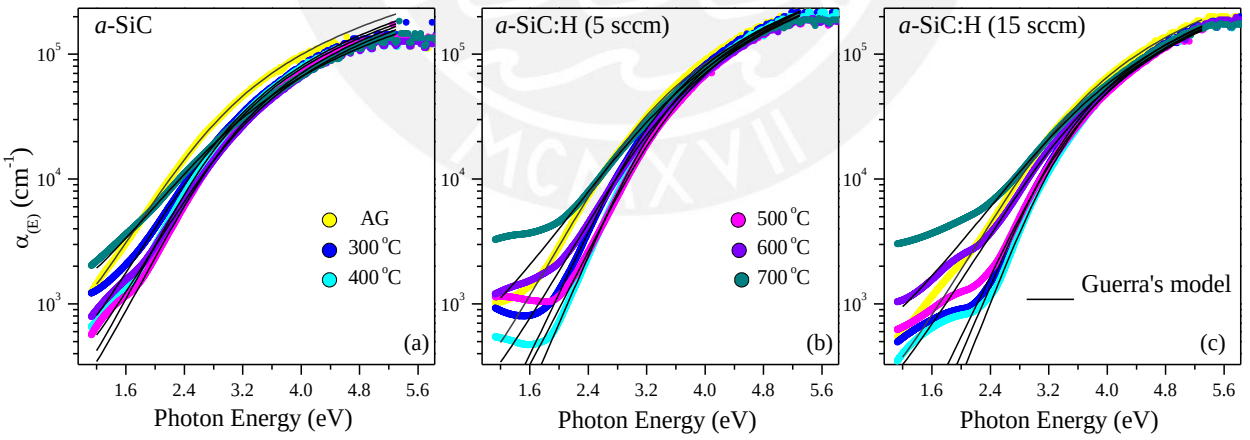

Figure 3.6 Optical absorption spectra $\alpha_{(E)}$ versus the photon energy, of *a*-SiC:H_x. The exhibited curves correspond to different annealing temperatures. The solid line is the Equation 2.38evaluated with the parameters obtained from a least squared fit. The color scheme is indicated in the legend within figure

It is found that the Di-logarithm function from Guerra's model is suitable to describe the optical behavior of the absorption coefficient of *a*-SiC:H, as shown in Figure 3.6. Following, the procedure in a-Si:H, the bandgap E_0 and E_u using the Guerra's model can be determine,

additionally, the Tau-gap from Tauc model and the tail breadth, E_u, from the Urbach rule, see Figure 3.7.

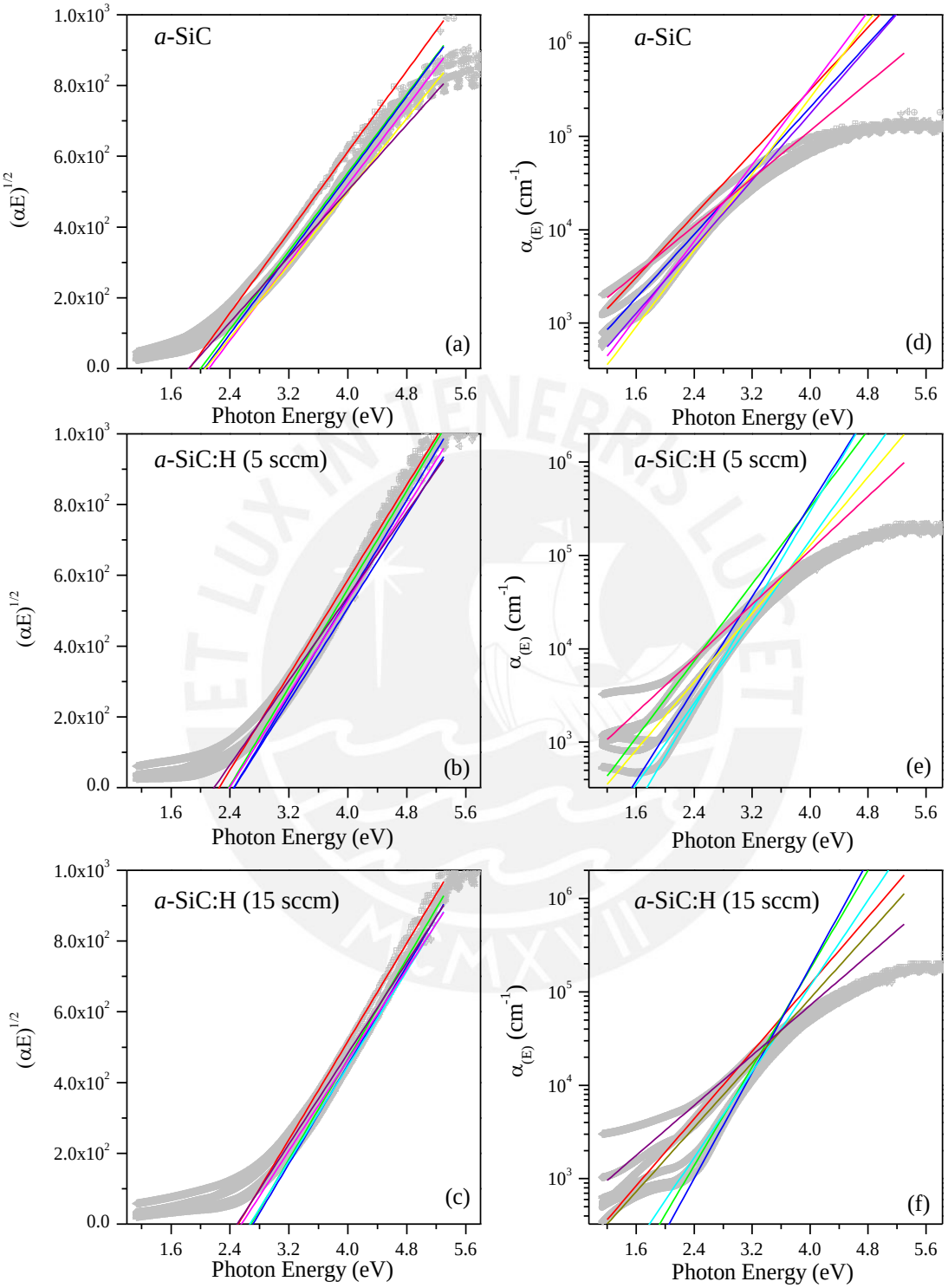

Figure 3.7 (a),(b) and (c)The Tauc plot. the Tauc is extrapolations corresponding for a-SiC and a-SiC:H$_x$ The data are depicted with the solid points, the least-squares fits to Tauc model being indicated with the solid lines. (d),(e)and (f) Urbach equation, the breadth of the optical absorption tail $E_u$by slope

3.3.1 The bandgap and Urbach energy of *a*-SiC:H_x

In reference to the analyzes the optical absorption spectrum corresponding to each *a*-SiC:H_x data set is characterized by determining the breadth of the optical absorption tail and corresponding optical gap. The effect of annealing temperature on the optical properties of *a*-SiC:H_x thin films were investigated. To begin, the structure of hydrogenated amorphous silicon carbide thin film present multiphase structure such as Si-C, C-C, C-H_n, Si-H_n [61]. Moreover, three different types of films polymethylsilane, polycarbosilane, and hydrogenated microcrystalline material are possible present from temperature effect [62].

The non-hydrogenated samples, the Tauc-gap increased with the annealing temperature up to 400ºC as shown in Figure 3.8 (a). It has been reported that the substrate temperature influences the growth of crystalline nanograins in *a*-SiC:H. In this manner, 200-300 ºC is the characteristic temperature at which the material is predominantly amorphous. However, Mohsen Daouahi et. al. [63] indicated the presence of nanocrystalline Si embedded in the amorphous SiC matrix. TEM studies revealed the presence of nanocrystallites in the films with size in the range of 2–10 nm [64]. Figure 3.8 (a) depicts the variation of the E_t. The E_u exhibits a trend that is opposite to that seen for the Tauc-gap, similarly to the observed in the *a*-Si:H case. Thereby, for the annealing temperatures between 500-700 ºC, E_t decreases, perhaps due to the strong connection between E_t and E_u. Now, the Urbach energy from the fit of the Urbach equation and Guerra's model. E_u decreases with increasing annealing temperature, up to 400 ºC. However, after 400 ºC annealing it increases. This could be related to the improving of carbon bonds [65]. Moreover, in the hydrogenated samples, it is possible that annealing at high temperatures results in evacuation of H around 500 ºC[66]; leads to an changes of structural disorder because of the increase of stress in the texture [67]

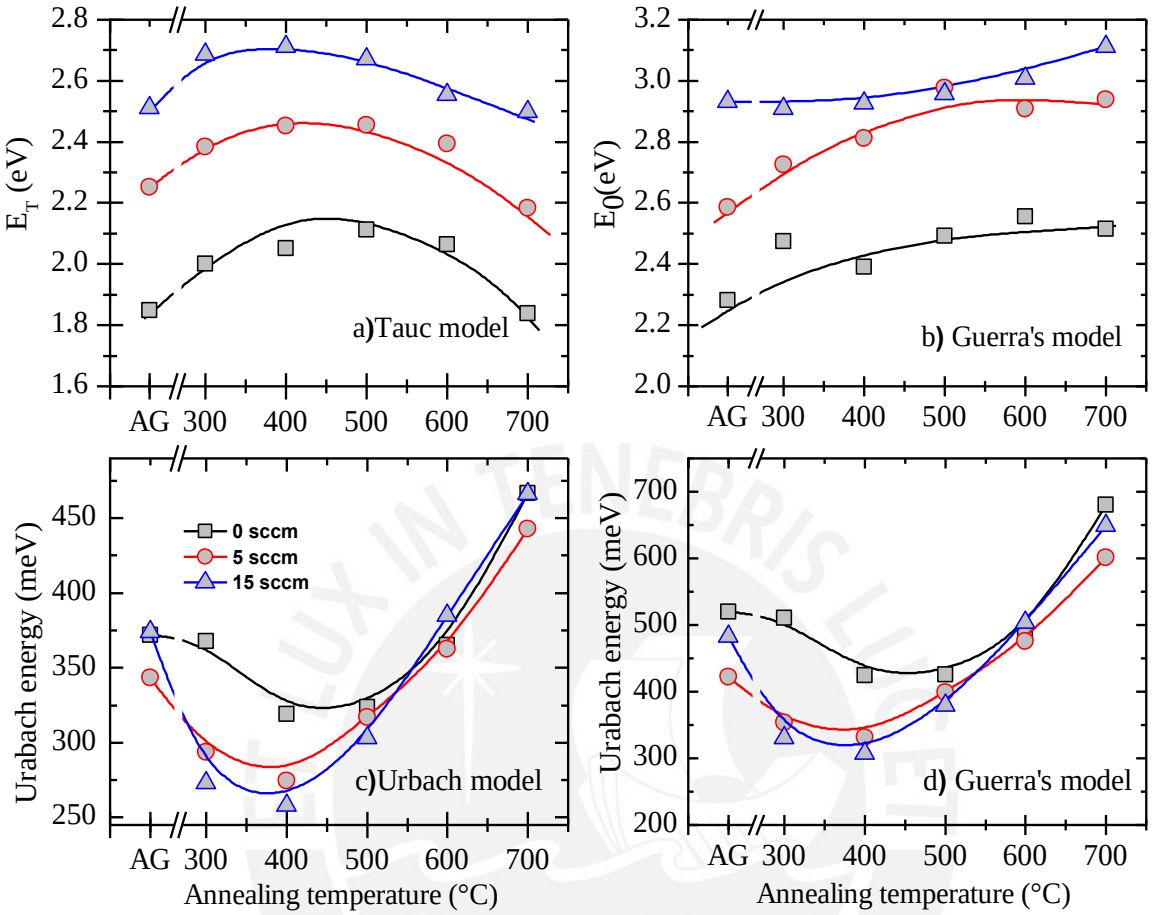

Figure 3.8 (a) Optical bandgap energies of a-SiC and a-SiC:H samples, from (a) the Tauc plots and from (b) Di-logarithm equation is square , E_0. (c) Urbach energies, from Urbach equation and (d) from Guerra's model

The optical bandgap of *a*-SiC:H is bigger than that of *a*-Si:H. In fact, the former increases with the incorporation of carbon atoms [19] [68]. In such case, the disorder degree increases with increasing carbon fraction [69]. The E_0 gap is independent of E_u as shown in figure 3.8. This fact is attributed to the definition of the E_0 bandgap from the Guerra model[1]. *a*-SiC exhibits a slow enhancement probably due to the increment of nanograins. These have been reported to form at 300 ºC [70]. This crystalline fraction increases about 60% when the substrate temperature is raised to 600 °C [70]. On the other hand, the E_0 gap changes slowly, see Figure 3.8 b. Additionally, the hydrogen incorporation enhances the E_0 value, from 2.586 to 2.938 eV for 5

sccm and from 2.931 to 3.110eV for 10 sccm. Following, Mohsen Daouahi et. al. [63] showed that at a substrate temperature of 400°C, and 500°C has a substantial change in the concentration of Si-C bonds, which increase which increasing of substrate temperature[63]. Then, it is may be the contribution to the bandgap, E_0,is related from SiC, SiC:H and clusters of Si and C crystalline with C-C bonds in sp^3 Hybridization[71][72].

3.4 Optical Characterization of amorphous Silicon-Nitride

Nitrogen atoms is an atom with a small ionic radius. Usually, the inclusion of smaller atoms into a semiconductor alloy that the material's bandgap increase, an effect of great significance for instance for the design of advanced solar cells [24]. Furthermore, it can be used as protective overcoats on magneto optical films and SiN film plays an important role for the passivation of silicon [25]. Now, the silicon nitride films were deposited by r.f. magnetron sputtering using a silicon nitride target at a low substrate temperate. High-purity Ar and N_2 were used and the temperature with a water cooling system at 10 °C to ensure the amorphous state of the films. A 51 mm diameter Si wafer were used as substrate[73]. It is significant to consider the oxygen absorption during film growth due it has been reported some vapors attributed to vacuum wall or substrates taking part in response in the sputtering process, or post annealing lead the oxygen may absorber by moisture[74]. Then, following similar procedure in *a*-Si:H and *a*-SiC:H. The bandgap E_0 and Urbach energy of the films were obtained by fitting the absorption coefficient data in the range 3.5–5.6 eV applying the Guerra´s model, Figure 3.9(a). The optical Tauc-gap and Urbach energy were deduced from the optical absorption by using the Tauc plots and Urbach model, in Figure 3.9 (b) and (c) is showed.

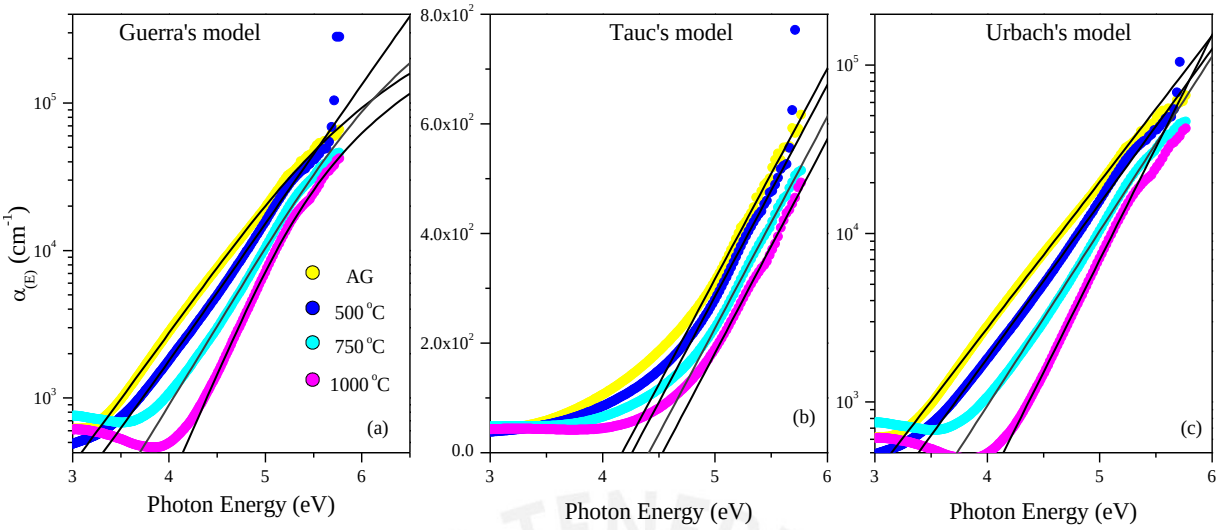

Figure 3.9 Optical absorption spectra $\alpha_{(E)}$ versus the photon energy, of a-SiN. The exhibited curves correspond to different annealing temperatures (a) Guerra's model, (b) Tauc plot and (b) Urbach's model.

In Figure 3.10 (a) shows the variation of the optical gap with the annealing temperature. As can be seen, the Tauc gap is as increasing function of the temperature. The measured values vary from 4.17 ± 0.01 eV, as growth, to 4.53 ± 0.01 at high temperature. These are of the same order of magnitude as those reported in [75], and this trend in the Tauc gap values has been also reported in [76]. Now, the film structure is a random mixture of bonds of Si-Si, Si-N rather than a mixture of segregated silicon and Si_3N_4 phases. Additionally, it has been previously reported that the reduction of Tauc gap is influenced by the decrease in Si and N bonds concentration in RF sputtering [77]. The Tauc gap increase may be due the nitrogen bonds [78] and strong connection with Urbach energy.

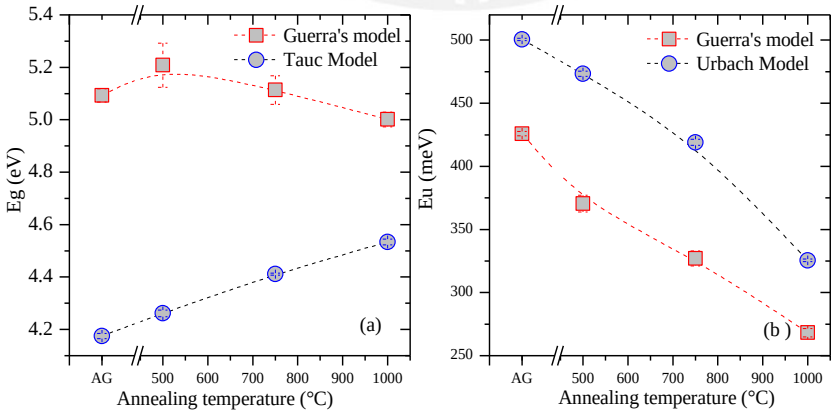

Figure 3.10(a) Optical bandgap energies of a-SiN samples, from the Tauc plots and from Guerra model. (b) Urbach energies, from Urbach equation and from Guerra's model

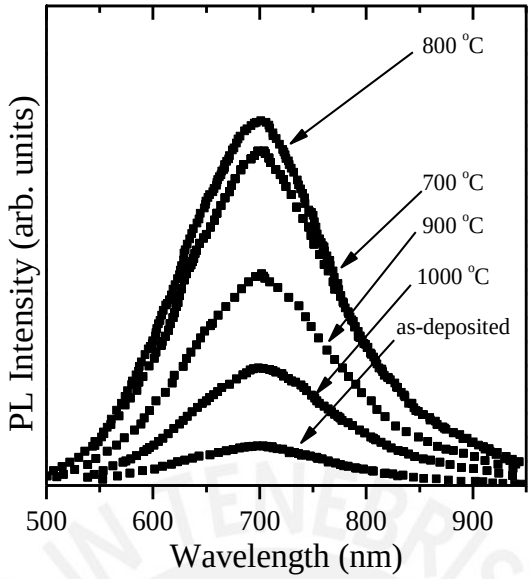

Figure 3.11 Photo Luminescence emission peak with temperature effect[79]

The optical bandgap can be controlled by varying the film stoichiometry[80]. Films with a silicon rich composition exhibit a Tauc-gap below 3 eV [81], in contrast, with films that present high Si-N bonds. The bandgap has been reported in range between 3.0 to 4.0 eV [75]. Here, as is shown in Figure 3.10 E_0 is around 5.15 eV for the whole temperature range. Changhun Ko et. al. [79] reported, by Photo Luminescence measurements that the host matrix related PL emission peak suffers a diminution if the FWHM due to annealing treatments, while a shift of the peak center when varying the nitrogen incorporation, Figure 3.11. it could be due to the fact that the mobility edge doesn't change considerably and, therefore, the E_0 value remains nearly constant. About the Urbach energy versus the annealing temperature. Jia Xiaoyun et al. studied structure of silicon nitride films deposited by r.f. magnetron sputtering and annealing treatment. According to his results, the bonds in the films emerged some fluctuates and the hydrogen concentration in the films after annealing decreased and the film presented a more compact construct [82], then it can be mainly reason of Urbach energy decrease.

3.5 Discussion of Urbach focus

The Urbach focus concept is applied to amorphous semiconductor materials by using the Urbach rule on optical absorption coefficient spectra[7] [43][50]. The Urbach focus is a constant found after modifying the disorder degree via for instance in situ temperature changes during the optical measurement or post-deposition thermal treatments. The disorder modification can be monitored by optical means through the Urbach energy. Our understanding as to how disorder influences the optical absorption spectrum gives way to the Urbach focus concept, which was defined as a parameter independent of static and thermal disorder. The notion was discussed in section 2.4, where the Urbach focus concept merely arose as an artifact of the particular fitting process or as an intrinsic property of the material. For this reason, four perspectives was covered: (i) the global fit method; (ii) the Cody relationship, derived from the interpretation of the Urbach Model; (iii) the Orapunt and O'Leary analysis, and (iv) our approach by asymptotic analysis using the dilogarithm equation from Guerra's model[1]. This matter was investigated with a critical examination and an appropriate model for the calculation of the Urbach focus. Therefore, it will be evaluated each model for *a*-Si:H, which has been reported extensively by many authors and contrast with our approach. Furthermore, also in *a*-SiC:H_x was studied in order to provide further validation to our model.

Urbach edges were studied in section 3.2.1 for *a*-Si:H, where the exponential slopes do not intersect at a local point but instead within a region around the Urbach focus (Figure 3.4 b).It is introduced the typical steps to find a local point or Urbach focus, by fitting different optical absorption spectra measurements using the Urbach model. First, the global fit method is applied, thereby, β by a least-squares fit can be determined and the parameters α_F and E_F are shared (are the same) for all these individual estimators from the Urbach equation, see section 2.4.1. The result shows that the Urbach focus occurs two to three decades beyond the Urbach region ($\alpha_F = 4.227 \times 10^6\ cm^{-1}\ \ E_F = 2.28\ eV$) on the absorption coefficient, which is shown in Figure 3.12. However, this is the first approach, in which two parameters (α_F, E_F) are shared. In the fitting process on the global fit method, it is may be enforced the Urbach existence or does not. For this reason, differently are proceed.

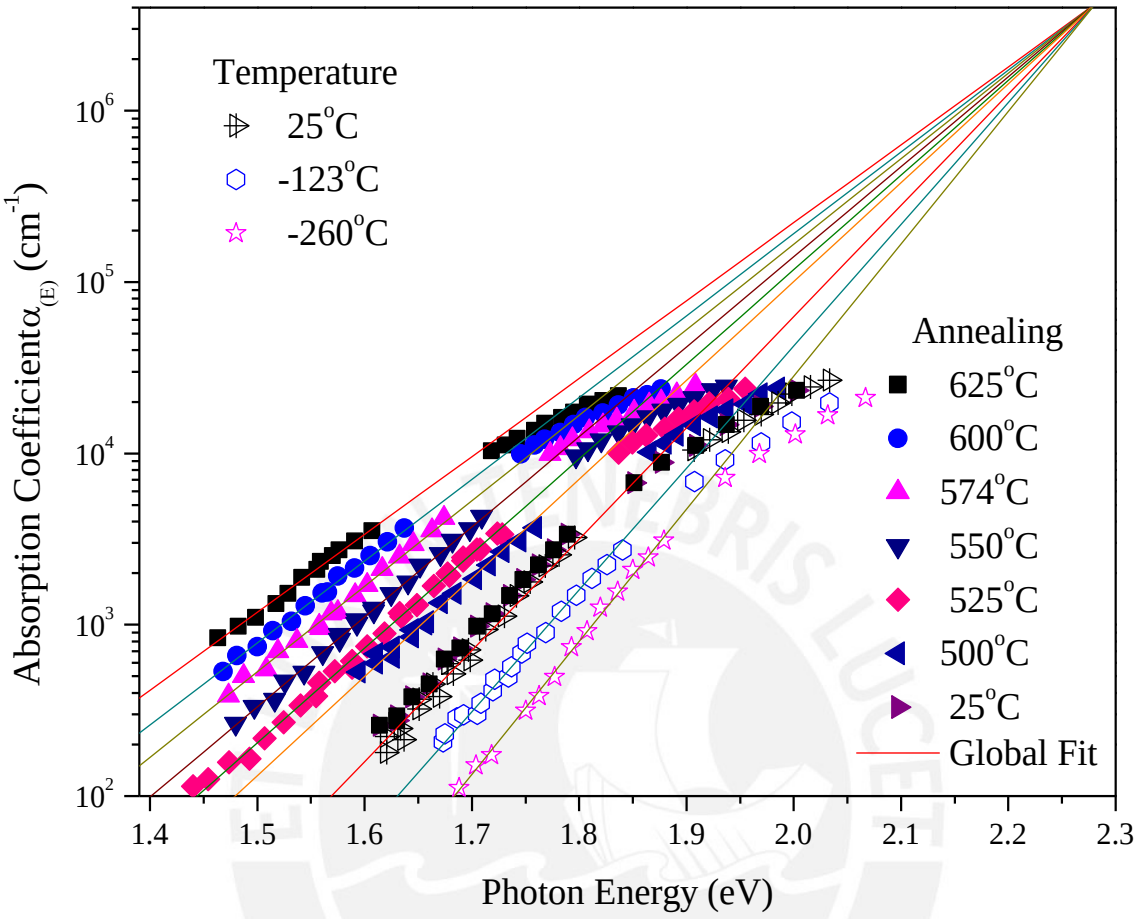

Figure 3.12 The Urbach focus find ($\alpha_F = 4.227 \times 10^6\ cm^{-1}$,$E_F = 2.28\ eV$) for the optical data corresponding to a-Si:H[47]*. Solid line are the fits to Urbach model using global fit method. The points represent experimental data for temperature and annealing effect.*

Cody found that the data of *a*-Si: H is consistent with the interpretation that the width of the exponential edge and the optical bandgap are influenced by the structural and thermal disorder amount [42]. Cody's analysis is performed. That is to test the linear relationship between Urbach energy and Tauc-gap derived from the interpretation of the Urbach energy (see section 2.4.2) [47]. That is, the optical bandgap decreases in response to an increase of the Urbach tail. In section 2.4.2, The Cody defined the Urbach focus [48] by, $E_F = E_g(X = 0, T = 0)$ for $E_U(X = 0, T = 0) = 0$. Thereby, the relationship can be expressed:

$$E_g(X,T) = E_F - G \times E_U(X,T) \qquad \textit{Equation 3.1}$$

Where, $E_g(X,T)$ is the optical bandgap to an amorphous semiconductor, E_F is Urbach focus, $E_U(X,T)$ is the Urbach energy, and G is a Cody constant. Following the procedure of Cody, it is considered the optical bandgap in amorphous semiconductor is equal the Tauc gap for *a*-Si:H

and E_u was found by independent fitting (the slope in Urbach region). Thereby, the linear relationship is found thus plotting Urbach energy and Tauc gap to *a*-Si:H, see Figure 3.13 (a). Then, the Equation 3.1 to find the Urbach focus as shown in Figure 3.13 (a).

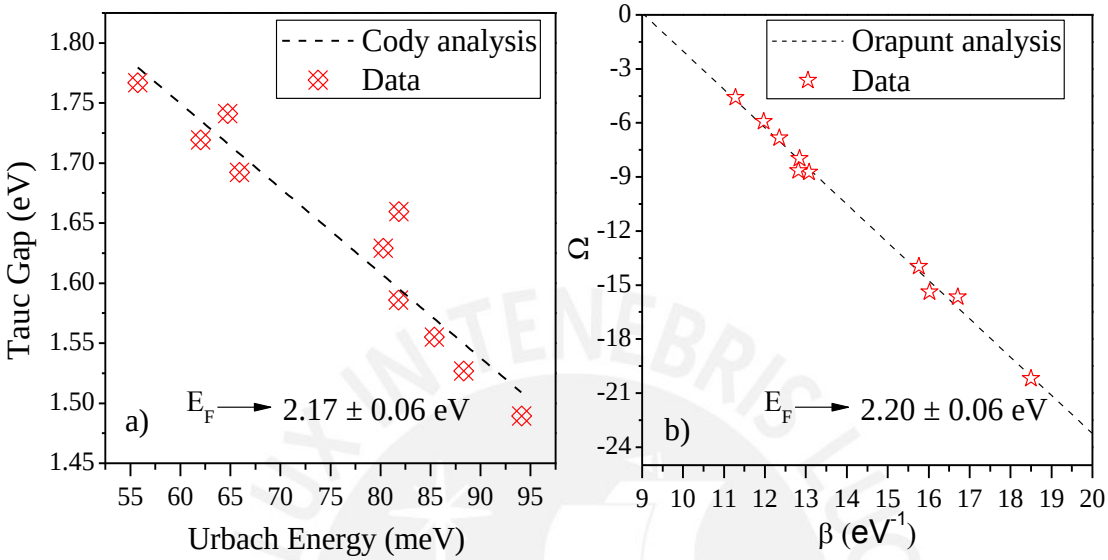

Figure 3.13 The Urbach focus find to the optical data corresponding to a-Si:H[47]. *In a) the Tauc gap and Urbach energy relationship by data cody and b)* Orapunt and O'leary *analysis working with Urbach equation.*

Another interesting alternative to understanding the Urbach focus concept was proposed by Orapunt and O'Leary's [49]. This analysis suggests to finding the parameter set (β, Ω), where β is the Urbach slope and Ω is the intercept in logarithm-scale of the Urbach rule and is also determined experimentally. Thenceforth the Urbach focus can be found by testing the linear relationship shown in equation 3.2.

$$\Omega = Ln(\alpha_F) - \beta E_F \qquad \textit{Equation 3.2}$$

The resulting linear fits are shown in Figure 3.13 (b). The Urbach focus found is equal to $2.20 \pm 0.06\, eV$. There is a striking similarity between the obtained values of E_F using the previously described models for the case of *a*-Si: H. The global fit may suggest that E_F merely arises as a mathematical artifact of the fitting process as in the global fit method. However, Cody and O'Leary have shown that a connection exists between the optical properties, such as Urbach

focus, of the materials by independent fit. As result the linear relationship in both methods (see Figure 3.13).

Finally, our model is employed following the asymptotic analysis in dilogarithm equation into the Urbach region. The parameter set (α_0, β, E_0) is determined by the least-square fit of dilogarithm equation that it was obtained by fitting data absorption coefficient of *a*-Si: H for each annealing (and temperature) step. Then, it is replace these parameters in Ψ as defined in Equation 3.3

$$\Psi = \ln\left[\frac{\pi}{4}\frac{\alpha_0}{\beta^2}\right] - \beta E_0 \qquad \textit{Equation 3.3}$$

$$\Psi = -\beta E_F + \ln[\alpha_F E_F] \qquad \textit{Equation 3.4}$$

Equation 3.4 was determined analytically in section 2.4.4. This linear relation between Ψ and β is shown in Figure 3.14 for *a*-Si:H. The slope lead to E_F = 2.22 $\pm$ 0.07 eV.

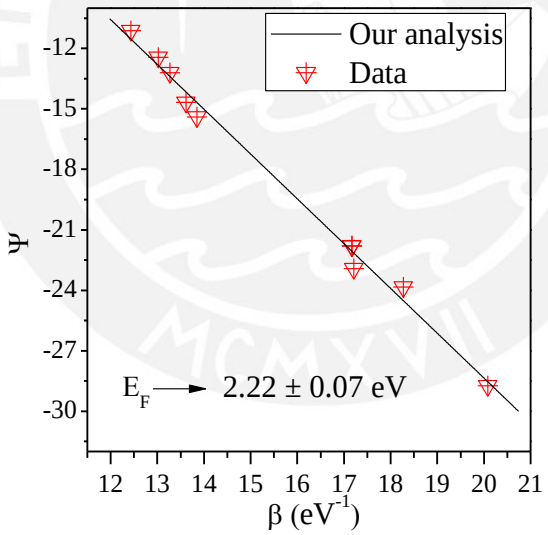

Figure 3.14 Linear fit of ψ vs β corresponding to the optical absorption of a-Si:H [47].

The Urbach focus for *a*-Si: H using the three methods through the data of Cody [Cody] is found. The obtained values are similar to each other (see table 3.1). Thenceforth, the same analysis on *a*-SiC:H_x will be applied. our model and other are tested to shed some light on the meaning of the Urbach focus [48].

Table 3.3 Urbach focus energy value for a-Si:H

	Our approach	**Orapunt approach**[49]	**Cody analysis**[47]
E_F	$2.22 \pm 0.07\ eV$	$2.20 \pm 0.06\ eV$	$2.17 \pm 0.06\ eV$

3.5.1 Urbach Focus of hydrogenated and non-hydrogenated amorphous silicon carbide.

Now the same analysis performed on *a*-Si: H is proceeded, moreover, on *a*-SiC:H grown with different hydrogen contents. Figure 3.15, depicts the global fit of the Urbach rule on the three samples. The Urbach focus obtained by a global fit is shown also shown in figure 3.12. The value is similar to that reported by F. Zhang et. al. [67]. Additionally, the existence of Urbach focus has been reported by J. A. Guerra et. al [12] Applying the global fit. The values for each hydrogen concentration are presented in the Table 3.4.

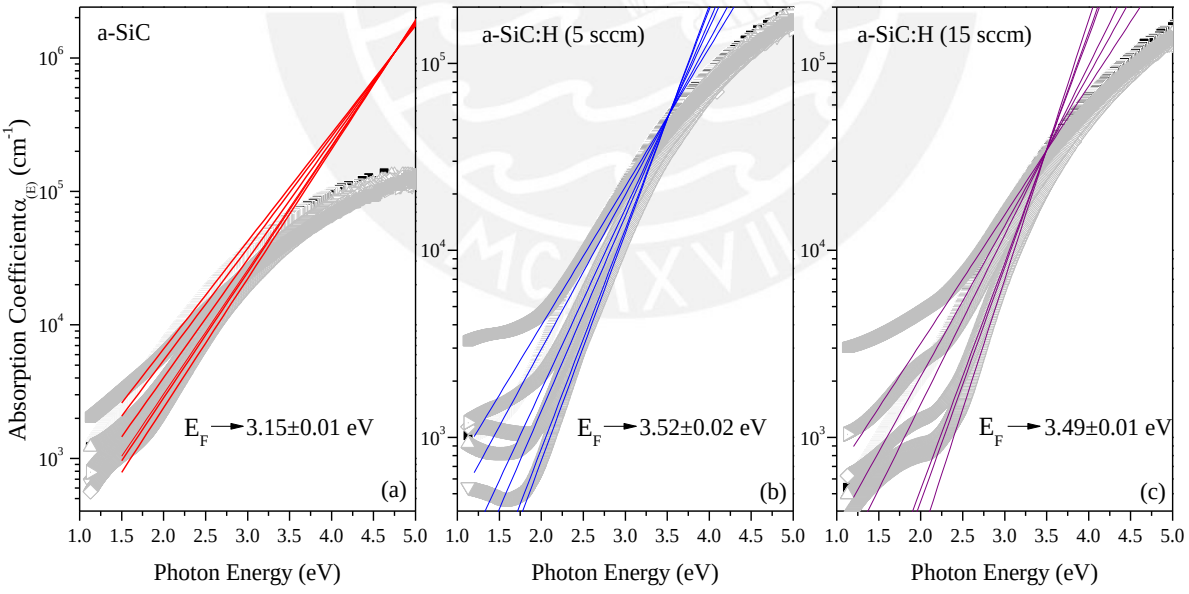

Figure 3.15 The Urbach focus find for the optical data corresponding to a-SiC, a-SiC:H (5 sccm) and a-SiC:H (15 sccm)[1]*. Solid line are the fits to Urbach model using global fit method. The points represent experimental data for annealing temperature effect.*

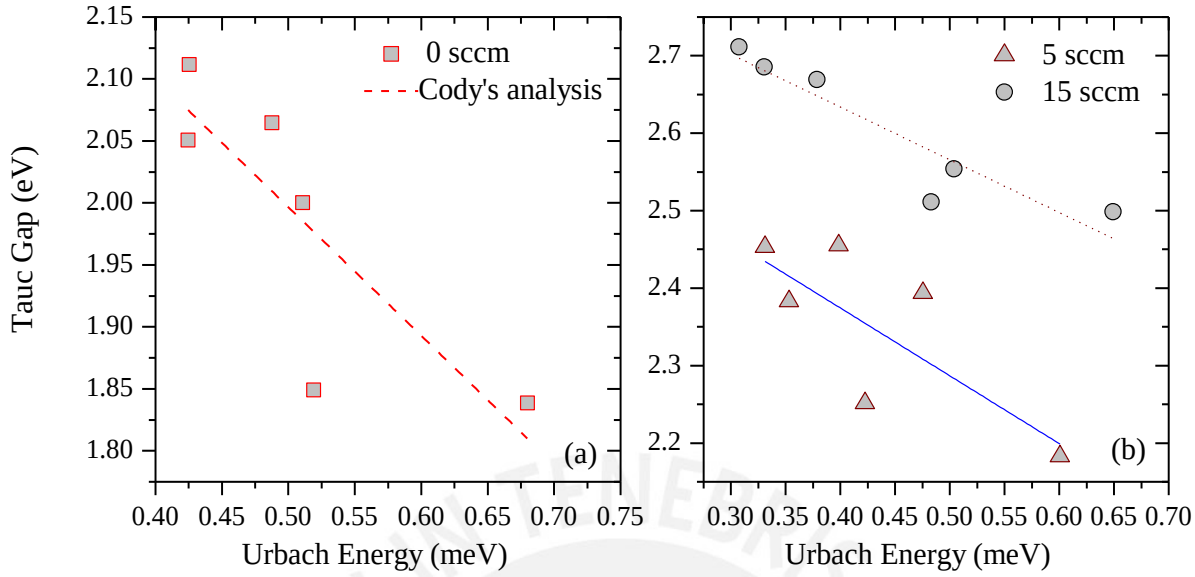

Figure 3.16 Linear fit using Equation 3.1 corresponding to the analysis of Cody for a) a-SiC, b) a-SiC:H

Through the relationship of Cody, it is obtained E_F and G. Whilst in the *a*-Si:H case a well defined linear behavior is observed between the Tauc-gap and the Urbach energy in the *a*-SiC:H case this does not happen. The dispersion between the data and linear equation is more evident (see Figure 3.16). For non-hydrogenated case *a*-SiC, presents evidence that different methods give rise to different Urbach focus energy values see table 3.4. On the other hand, the hydrogen incorporation establishes lower dispersion within this linear relation. Nevertheless, the global fit predicts slightly different values for the Urbach focus energy coordinate.

The Orapunt analysis was performed. That is, performing independent linear fits in Urbach region of the logarithm of the absorption coefficient *a*-SiC and *a*-SiC :H, which has been fully studied by J. A. Guerra [12]. Essentially, those materials show a linear relation agreeing with Orapunt and O'Leary found for *a*-Si:H [49]. The values of the Urbach focus obtained through the aforementioned methods are shown in Table 3.4. Notice that following our approach, the expected linear behavior is met with a much lower dispersion than the Orapunt analysis as shown in Figure 3.17 (a) and (b).

The three performed analysis revealed that the experimental data are consistent with the notion of the Urbach focus concept. Now, the validity of the Urbach focus for *a*-SiC:H will be critically

examined, based on our analysis. Figure 3.17 depicts the lineal dependence of Ψ and β for non-hydrogenated (c) and hydrogenated (d) *a*-SiC. Note that the experimental data exhibits quite a linear behavior. The procedure to find the coordinates (β,Ψ) was explained for the case of *a*-Si:H. Thenceforth, a linear least squares fit this experimental data allowed us to determinate the slope (E_F) of Equation 3.4, and the intercept (Ln[α_F]). This result is contrasted with that obtained by the analysis of Orapunt and O'leary applied in the same materials. Table 3.4 summarizes these results.

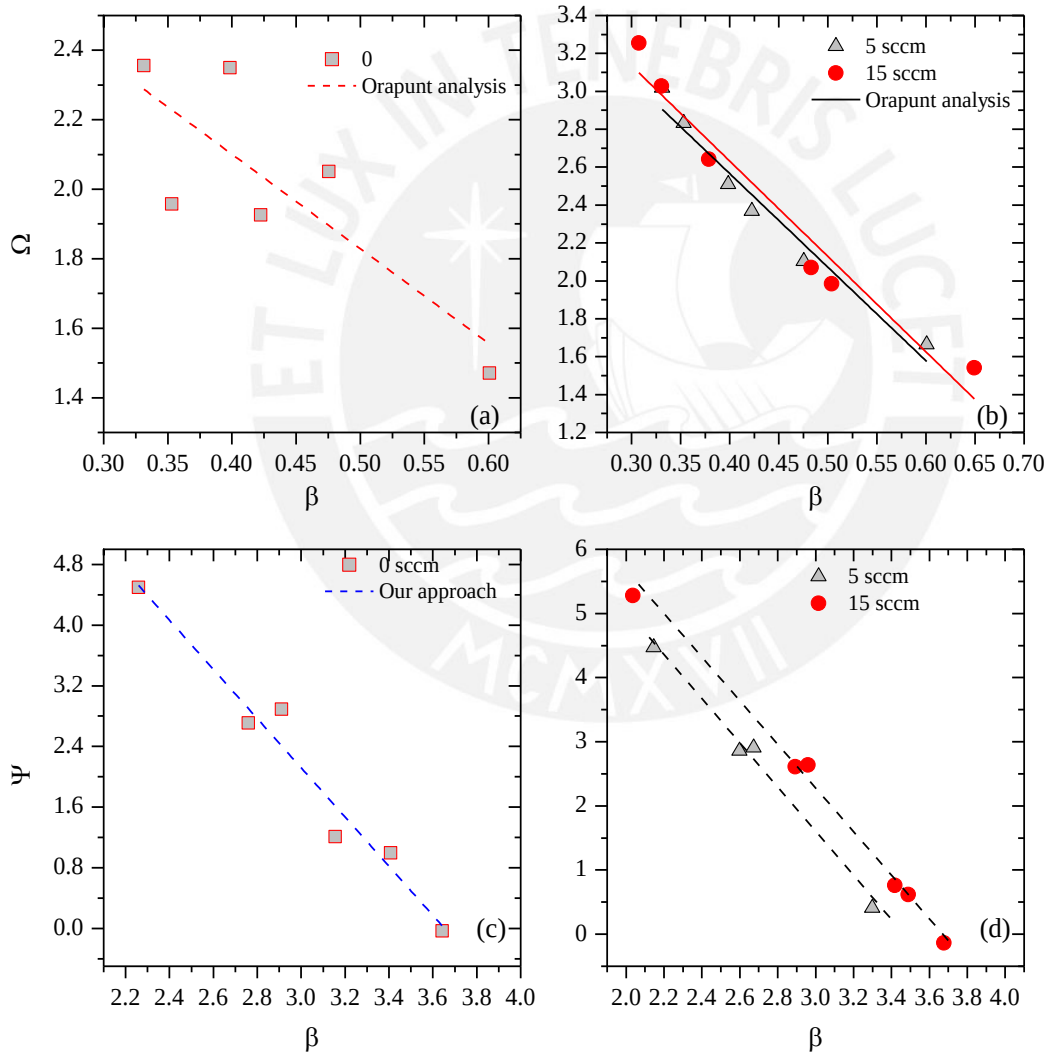

Figure 3.17 Urbach focus using Orapunt approach by the linear dependence of Ω on beta for a) a-SiC, b) a-SiC:H and using our approach by the linear dependence of Ψ on beta for (c) a-SiC, (d) a-SiC:H

Table 3.4. Urbach Focus of hydrogenated and non-hydrogenated amorphous silicon carbide.

Material		Parameter	Global fit	Cody Relationship	Orapunt Analysis	Our analysis
***a*-SiC**		$\ln[\alpha_F]$	10.48±0.02	---	10.48 ± 1.17	10.94 ± 0.44
		E_F (eV)	**3.15±0.01**	**2.50 ± 0.18**	**3.09 ± 0.57**	**3.31 ± 0.12**
***a*-SiC:Hx**	5 sccm	$\ln[\alpha_F]$	10.89±0.05	---	10.08 ± 0.47	10.68 ± 0.96
		E_F (eV)	**3.52±0.02**	**2.73 ± 0.16**	**3.06 ± 0.26**	**3.24 ± 0.03**
	15 sccm	$\ln[\alpha_F]$	10.43±0.01	---	10.38 ± 0.27	10.68 ± 0.31
		E_F (eV)	**3.49±0.01**	**2.91 ± 0.06**	**3.45 ± 0.12**	**3.45 ± 0.09**

Finally, notice that the values of the Urbach focus found under the Orapunt and O'Leary analysis have a similar behavior to the values found in our analysis in *a*-SiC, *a*-SiC:H_x. On the contrary, Cody's relationship present differences for 5 sccm in from of other models, see Table 3.4. In Figure 3.18 depicts the Urbach focus energy ordinate found by the three analysis. The Urbach focus presents an enhancement, with the hydrogen incorporation. Most likely due to the decrease of dangling bonds and, therefore, the shrinking of the mean lattice parameter. This result suggests a direct connection between the mobility edges and the Urbach focus.

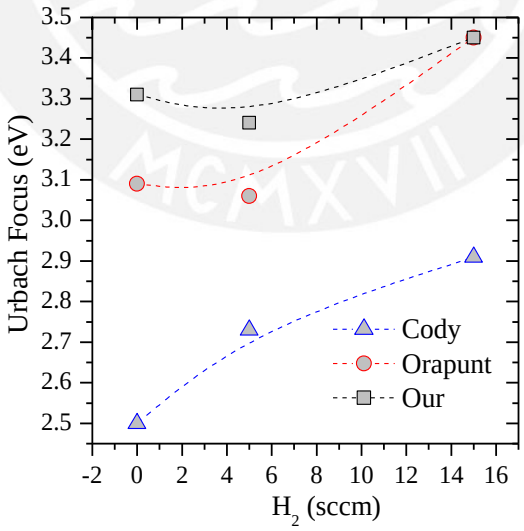

Figure 3.18 The Urbach focus energy ordinate found by the three approaches

4. Conclusions and outlook

In the present work distinct approaches to describe the fundamental absorption of amorphous semiconductors have been reviewed. Three models: Tauc, Urbach and Guerra, were evaluated. These models were used to fit the absorption coefficient data of *a*-Si:H, *a*-SiC:H and a-SiN. With a single fit the bandgap in the absence of disorder and the Urbach energy were simultaneously obtained. The spectral region where the Tauc and Urbach tail absorption overlap was also used in the aforementioned single fit. This is in contrast to the traditional models, which required a separation of the optical absorption in these two regions in order to perform the corresponding analysis.

Before applying Guerra's model on the experimental absorption coefficient data, it was evaluated how variations in the Urbach energy influenced the shape of the Di-Logarithm function. In this sense, the capability of this model to fit generated data of the absorption coefficient and to obtain relevant parameters through simulation was tested. It was possible to recover the parameter E_0 and it was found that it is independent of the disorder degree as shown by simulations. Furthermore, the results on the experimental data also confirm the independency of E_0 on the Urbach energy. Additionally, the Tauc-gap and the Urbach energy showed a linear relationship which was described by the model of Cody.

In the case of *a*-Si:H, the E_0 and the Tauc gaps showed a similar behavior with the annealing temperature. This behavior is mainly attributed to the fact that the chemistry changes as soon as the hydrogen concentration decreases. Thereby, on the one hand, E_0 diminishes suggesting a diminution of the energy separation between the mobility edges. On the other hand, the Urbach energy increases with the annealing temperature, due to the increasing stress in the lattice induced by the hydrogen loss.

In the case of *a*-SiC:H_x, the changes observed in E_0 after annealing do not follow the behavior of the Tauc-gap: First, the Urbach energy demonstrated a shrinking with an increasing annealing temperature. Then, after a critical temperature of 400°C, an increase

was observed. A possible explanation for the latter observation could be the formation of clusters of Si and C in the films at this critical temperature and above.

In the case of *a*-SiN, E_0 exhibits a nearly constant behavior with the annealing temperature. This result suggests that the mobility edges do not change considerably under thermal annealing treatments. Additionally, it was shown that E_0 and E_u also demonstrate an independent behavior from one another.

Even though the model proposed by J. A. Guerra does not predict an Urbach focus, this concept is compatible with it. An analysis was developed that allows the measurement of the Urbach focus energy ordinate (E_F) based on the model of Guerra. The Urbach focus of the two materials *a*-Si:H and *a*-SiC:H under the approach of Orapunt and by our analysis were found. In these cases the Cody approach did not result in a well-defined linear behavior. In this sense, it is recommended to use our approach or Orapunt's analysis to determine the Urbach focus.

Finally, an interesting feature was observed in the case of *a*-SiC:H grown with different hydrogen contents: An increase of the Urbach focus energy ordinate with an increase of the hydrogen incorporation during the deposition process was observed. This behavior correlates with the increase of the band-edge energy separation as it was shown in the recovered E_0 value. Part of these results have been recently published [1].

In order to validate the Guerra's model, it is recommended first to apply the method to other amorphous semiconductors materials. Additional information of the band-to-band transition and tail-to-band transitions can be provided by alternative techniques. For instance, through photo-luminescence measurements. Finally, the role of the Urbach focus in amorphous semiconductors could be interpreted by changes of the chemistry as shown in the case of *a*-SiC:H_x with distinct hydrogen contents.

References

[1] J. A. Guerra, J. R. Angulo, S. Gomez, and J. Llamoza, "The Urbach focus and optical properties of amorphous hydrogenated SiC thin films," *J. Phys. D. Appl. Phys.*, pp. 1–10, 2016.

[2] J. J. Thevaril, "The Optical Response of Hydrogenated Amorphous Silicon," University of Windsor, 2011.

[3] B. Abeles, "Exponential absorption edge in hydrogenated α-Si films," *Solid State Commun.*, vol. 36, no. 6, pp. 537–540, 1980.

[4] R. A. Street, *Hydrogenated amorphous silicon*, no. 2. New York, 1991.

[5] J. Tauc, R. Grigorovici, and A. Vancu, "Optical Properties and Electronic Structure of Amorphous Germanium," *Phys. Status Solidi*, vol. 15, no. 2, pp. 627–637, 1966.

[6] F. Urbach, "The long-wavelength edge of photographic sensitivity and of the electronic Absorption of Solids," *Phys. Rev.*, vol. 92, no. 5, p. 1324, 1953.

[7] T. H. Keil, "Theory of the urbach rule," *Phys. Rev.*, vol. 144, no. 2, pp. 582–587, 1966.

[8] W. C. Chen, B. J. Feldman, J. Bajaj, F. M. Tong, and G. K. Wong, "'Thermalization gap' excitation photoluminescence and optical absorption in amorphous silicon-hydrogen alloys," *Solid State Commun.*, vol. 38, no. 5, pp. 357–363, 1981.

[9] D. Redfield, "Energy-band tails and the optical absorption edge; the case of a-si:H," *Solid State Cormnunications*, vol. 44, pp. 1347–49, 2014.

[10] S. K. O'Leary, "On the relationship between the distribution of electronic states and the optical absorption spectrum in amorphous semiconductors," *Solid State Commun.*, vol. 109, no. 9, pp. 589–594, 1999.

[11] C. M. Soukoulis, M. H. Cohen, and E. N. Economou, "Exponential Band Tails in Random Systems," *Phys. Rev. Lett.*, vol. 53, no. 6, pp. 616–619, 1984.

[12] A. W. and W. J.A. Guerra, L. Montañes. F. De Zela, “On the Origin of the Urbach rule and the Urbach Focus,” *MRS*, 2013.

[13] C.-Y. Ho and Y.-J. Chang, “Effects of various gate materials on electrical degradation of a-Si:H TFT in industrial display application,” *Solid. State. Electron.*, 2015.

[14] M.-Y. Tsai, T.-C. Chang, A.-K. Chu, T.-Y. Hsieh, K.-Y. Lin, Y.-C. Wu, S.-F. Huang, C.-L. Chiang, P.-L. Chen, T.-C. Lai, C.-C. Lo, and A. Lien, “Anomalous degradation behaviors under illuminated gate bias stress in a-Si:H thin film transistor,” *Thin Solid Films*, vol. 572, pp. 79–84, 2014.

[15] V. Gradišnik and A. Linić, “Defects characterization in p-i-n a-Si:H photodiode i-layer,” *J. Non. Cryst. Solids*, vol. 363, pp. 193–198, 2013.

[16] M. Mikolášek, M. Nemec, J. Kováč, M. Foti, C. Gerardi, G. Mannino, L. Valenti, and S. Lombardo, “The influence of post-deposition annealing upon amorphous silicon/crystalline silicon heterojunction solar cells,” *Mater. Sci. Eng. B Solid-State Mater. Adv. Technol.*, vol. 189, pp. 1–6, 2014.

[17] X. Zhang, A. Cuevas, B. Demaurex, and S. De Wolf, “Sputtered Hydrogenated Amorphous Silicon for Silicon Heterojunction Solar Cell Fabrication,” *Energy Procedia*, vol. 55, pp. 865–872, 2014.

[18] S. Kamiyama, M. Iwaya, T. Takeuchi, I. Akasaki, R. Yakimova, and M. Syväjärvi, “White light-emitting diode based on fluorescent SiC,” *Thin Solid Films*, vol. 522, pp. 23–25, 2012.

[19] Y. Tawada, H. Okamoto, and Y. Hamakawa, “A-SiC:H/a-Si:H heterojunction solar cell having more than 7.1% conversion efficiency,” *Appl. Phys. Lett.*, vol. 39, no. 3, pp. 237–239, 1981.

[20] T. Ma, J. Xu, J. Du, W. Li, X. Huang, and K. Chen, “Full color light emission from amorphous SiCx:H with organic–inorganic structures,” *J. Appl. Phys.*, vol. 88, no. 11, p. 6408, 2000.

[21] K. J. Roe, G. Katulka, J. Kolodzey, S. E. Saddow, and D. Jacobson, “Silicon carbide and silicon carbide:Germanium heterostructure bipolar transistors,” *Appl. Phys. Lett.*, vol. 78, no. 14, pp. 2073–2075, 2001.

[22] M. Kunii, K. Hasegawa, H. Oka, Y. Nakazawa, T. Takeshita, and H. Kurihara, "Performance of a High-Resolution Contact-Type Linear Image Sensor with a-Si: H/a-SiC: H Heterojunction Photodiodes," *IEEE Trans. Electron Devices*, vol. 36, no. 12, pp. 2877–2882, 1989.

[23] D. Klein and M. Kunst, "Study of surface passivation of crystalline silicon with amorphous silicon carbide deposited by plasma enhanced chemical vapor deposition," *Appl. Phys. Lett.*, vol. 99, no. 23, pp. 3–6, 2011.

[24] Z. Zhu, H. Shao, X. Dong, N. Li, B.-Y. Ning, X.-J. Ning, L. Zhao, and J. Zhuang, "Electronic Band Structure and Sub-band-gap Absorption of Nitrogen Hyperdoped Silicon," *Sci. Rep.*, vol. 5, p. 10513, 2015.

[25] S. K. Ghosh and T. K. Hatwar, "Preparation and characterization of reactively sputtered silicon nitride thin films," *Thin Solid Films*, vol. 166, no. C, pp. 359–366, 1988.

[26] C. Kittel, "Introduction to solid state physics." Library of congress cataloging, 1976.

[27] G. Auletta, M. Fortunato, and G. Parisi, *Quantum Mechanics*. 2009.

[28] J. J. Sakurai, *Modern Quantum Mechanics, Revised Edition*, vol. 63, no. 1. 1995.

[29] K. . Hass and H. Ehrenreich, "Electronic structure models, bonding, and optical moments in amorphous and crystalline semiconductors," *Ann. Phys. (N. Y).*, vol. 164, no. 1, pp. 77–102, 1985.

[30] J. and B. B. Patterson, *Solid-State Physics*, no. 1. 2014.

[31] J. Singh and K. Shimakawa, "Advances in Amorphous Advances in condensed matter science," *Structure*.

[32] M. Stutzmann, "The defect density in amorphous silicon," *Philos. Mag. Part B*, vol. 60, no. 4, pp. 531–546, 1989.

[33] S. K. O'Leary and P. K. Lim, "On determining the optical gap associated with an amorphous semiconductor: A generalization of the Tauc model," *Solid State Commun.*, vol. 104, no. 1, pp. 17–21, 1997.

[34] G. D. Cody, *Hydrogenated Amorphous Silicon - Optical Properties*, vol. 21. 1984.

[35] L. Jiao, I. Chen, R. W. Collins, C. R. Wronski, and N. Hata, "An improved analysis for band edge optical absorption spectra in hydrogenated amorphous silicon from optical and photoconductivity measurements," *Appl. Phys. Lett.*, vol. 72, no. 9, pp. 1057–1059, 1998.

[36] A. Ibrahim and S. K. J. Al-Ani, "Models of optical absorption in amorphous semiconductors at the absorption edge - A review and re-evaluation," *Czechoslov. J. Phys.*, vol. 44, no. 8, pp. 785–797, 1994.

[37] A. P. Sokolov, A. P. Shebanin, O. A. Golikova, and M. M. Mezdrogina, "Structural disorder and optical gap fluctuations in amorphous silicon," *J. Phys. Condens. Matter 3*, vol. 3, no. 49, pp. 9887–9894, 1991.

[38] E. Freeman and W. Paul, "Optical constants of rf sputtered hydrogenated amorphous Si," *Phys. Rev. B*, vol. 20, no. 2, pp. 716–728, 1979.

[39] J. Müllerová, L. Prušáková, M. Netrvalová, V. Vavruňková, and P. Šutta, "A study of optical absorption in amorphous hydrogenated silicon thin films of varied thickness," *Appl. Surf. Sci.*, vol. 256, pp. 5667–5671, 2010.

[40] J. Müllerová and V. Vavruˇ nková, "Optical absorption in PECVD deposited thin hydrogenated silicon in light of ordering effects," *Cent. Eur. J. Phys.*, vol. 7, no. 2, pp. 315–320, 2009.

[41] I. a Weinstein, a F. Zatsepin, and V. S. Kortov, "Effects of structural disorder and Urbach ' s rule in binary lead silicate glasses," *J. Non. Cryst. Solids*, vol. 279, pp. 77–87, 2001.

[42] G. D. Cody, T. Tiedje, B. Abeles, B. Brooks, and Y. Goldstein, "Disorder and the optical-absorption edge of hydrogenated amorphous silicon," *Phys. Rev. Lett.*, vol. 47, no. 20, pp. 1480–1483, 1981.

[43] M. Kranjčec, I. P. Studenyak, and M. V. Kurik, "On the Urbach rule in non-crystalline solids," *J. Non. Cryst. Solids*, vol. 355, no. 1, pp. 54–57, 2009.

[44] I. I. Shpak and I. P. Studenyak, "Optical Absorption Edge and Structural Disorder," *J. Optoelectron. Adv. Mater.*, vol. 5, no. 5, pp. 1135 – 1138, 2003.

[45] J. . and S. R. . Howard, “Evidence for potential fluctuationes in compensated amorphous silicon,” *Phys. Rev. B*, vol. 27, no. 13008, pp. 325–339, 1973.

[46] L. M. Montañez, J. A. Guerra, K. Zegarra, S. Kreppel, F. De Zela, A. Winnacker, and R. Weingärtner, “Optical bandgap enhancement of a -SiC through hydrogen incorporation and thermal annealing treatments,” *Proc. SPIE - Int. Soc. Opt. Eng.*, vol. 8785, p. 87859S, 2013.

[47] G. D. Cody, “Urbach edge of cristalline and amorphous silicon: a personal review,” *J. Non. Cryst. Solids*, vol. 141, pp. 3–15, 1992.

[48] G. D. Cody, “Urbach Edge , Disorder , and Absorption On-set in a-Si : H,” *Mater. Res. Soc.. Symp. Proc.*, vol. 862, no. 4, pp. 1–13, 2005.

[49] F. Orapunt and S. K. O’Leary, “The Urbach focus and hydrogenated amorphous silicon,” *Appl. Phys. Lett.*, vol. 84, no. 4, p. 523, 2004.

[50] B. Jarza, J. Weszka, J. Cisowski, and L. Bryja, “Influence of temperature on the optical absorption edge in amorphous Zn–P thin films,” pp. 554–557, 1998.

[51] S. K. O’Leary, S. Zukotynski, and J. M. Perz, “Disorder and optical absorption in amorphous silicon and amorphous germanium,” *J. Non. Cryst. Solids*, vol. 210, no. 2–3, pp. 249–253, 1997.

[52] D. E. Sweenor, S. K. O’Leary, and B. E. Foutz, “On defining the optical gap of an amorphous semiconductor: An empirical calibration for the case of hydrogenated amorphous silicon,” *Solid State Commun.*, vol. 110, no. 5, pp. 281–286, 1999.

[53] T. A. Abtew, F. Inam, and D. A. Drabold, “Thermally stimulated H emission and diffusion in hydrogenated amorphous silicon,” *Europhys. Lett.*, vol. 79, no. 3, p. 4, 2006.

[54] Y. Abdulraheem, I. Gordon, T. Bearda, H. Meddeb, and J. Poortmans, “Optical bandgap of ultra-thin amorphous silicon films deposited on crystalline silicon by PECVD,” *AIP Adv.*, vol. 4, no. 5, p. 057122, 2014.

[55] G. Müller, G. Krötz, S. Kalbitzer, and G. N. Greaves, “Reversible and irreversible structural changes in amorphous silicon,” *Philosophical Magazine Part B*, vol. 69, no. 2. pp. 177–196, 1994.

[56] P. K. Sarswat and M. L. Free, "A Study of Energy Band Gap Temperature Relationships for Cu2ZnSnS4 Thin Films," *Phys. Status Solidi Appl. Mater. Sci.*, vol. 208, no. 12, pp. 2861–2864, 2011.

[57] Y. Laaziz, a Bennouna, and E. Ameziane, "The effect of annealing on the optical and electrical properties of a-Si:H sputtered films," *Sol. Energy Mater. Sol. Cells*, vol. 31, no. 1, pp. 23–32, 1993.

[58] P. D. Persans, A. F. Ruppert, S. S. Chan, and G. D. Cody, "Relationship between bond angle disorder and the optical edge of aGe:H," *Solid State Commun.*, vol. 51, no. 4, pp. 203–207, 1984.

[59] W. B. Amer, Nabil M and Jackson, "Optical properties of defect states in a-Si: H," *Semicond. Semimet. B*, vol. 21, pp. 83–112, 1984.

[60] J. J. Thevaril and S. K. O'Leary, "The role that conduction band tail states play in determining the optical response of hydrogenated amorphous silicon," *Solid State Commun.*, vol. 151, no. 9, pp. 730–733, 2011.

[61] Y. . Wang, J. Lin, and C. H. . Huan, "Multiphase structure of hydrogenated amorphous silicon carbide thin films," *Mater. Sci. Eng. B*, vol. 95, no. 1, pp. 43–50, 2002.

[62] M. Lee, "Temperature effects in the hot wire chemical vapor deposition of amorphous hydrogenated silicon carbon alloy," *J. Appl. Phys.*, vol. 87, no. 9, p. 4600, 2000.

[63] M. Daouahi and N. Rekik, "Effect of Substrate Temperature on (Micro/Nano) Structure of a-SiC:H Thin Films Deposited by Radio-Frequency Magnetron Sputtering. Mohsen," *Phys. Chemestry C*, vol. 116, pp. 21018–26, 2012.

[64] T. Rajagopalan, X. Wang, B. Lahlouh, C. Ramkumar, P. Dutta, and S. Gangopadhyay, "Low temperature deposition of nanocrystalline silicon carbide films by plasma enhanced chemical vapor deposition and their structural and optical characterization," *J. Appl. Phys.*, vol. 94, no. 8, pp. 5252–5260, 2003.

[65] J. Cui, S. F. Yoon, M. B. Yu, K. Chew, J. Ahn, Q. Zhang, E. J. Teo, T. Osipowicz, and F. Watt, "Effects of microwave power on the structural and emission properties of hydrogenated amorphous silicon carbide deposited by electron cyclotron resonance chemical vapor deposition," *J. Appl. Phys.*, vol. 89, no. 5, p. 2699, 2001.

[66] Y.-T. Kim, S.-M. Cho, B. Hong, S.-J. Suh, G.-E. Jang, and D.-H. Yoon, "Annealing Effect on the Optical Properties of a-SiC:H Films Deposited by PECVD.," *Mater. Trans.*, vol. 43, no. 8, pp. 2058–2062, 2002.

[67] F. Zhang, H. Xue, Z. Song, and Y. Guo, "Effect of high-temperature annealing on the optical-absorption edge of hydrogenated amorphous silicon-carbon films," vol. 46, no. 8, pp. 4590–4594, 1992.

[68] J. P. Conde, V. Chu, M. F. da Silva, a. Kling, Z. Dai, J. C. Soares, S. Arekat, a. Fedorov, M. N. Berberan-Santos, F. Giorgis, and C. F. Pirri, "Optoelectronic and structural properties of amorphous silicon–carbon alloys deposited by low-power electron-cyclotron resonance plasma-enhanced chemical-vapor deposition," *J. Appl. Phys.*, vol. 85, no. 6, p. 3327, 1999.

[69] K. Chew, Rusli, S. F. Yoon, J. Ahn, V. Ligatchev, E. J. Teo, T. Osipowicz, and F. Watt, "Hydrogenated amorphous silicon carbide deposition using electron cyclotron resonance chemical vapor deposition under high microwave power and strong hydrogen dilution," *J. Appl. Phys.*, vol. 92, no. 5, pp. 2937–2941, 2002.

[70] S. Kerdiles, a. Berthelot, F. Gourbilleau, and R. Rizk, "Low temperature deposition of nanocrystalline silicon carbide thin films," *Appl. Phys. Lett.*, vol. 76, no. 17, p. 2373, 2000.

[71] C. Summonte, R. Rizzoli, M. Bianconi, a. Desalvo, D. Iencinella, and F. Giorgis, "Wide band-gap silicon-carbon alloys deposited by very high frequency plasma enhanced chemical vapor deposition," *J. Appl. Phys.*, vol. 96, no. 7, pp. 3987–3997, 2004.

[72] H. Schmidt, E. R. Fotsing, G. Borchardt, R. Chassagnon, S. Chevalier, and M. Bruns, "Crystallization kinetics of amorphous SiC films: Influence of substrate," *Appl. Surf. Sci.*, vol. 252, no. 5, pp. 1460–1470, 2005.

[73] J. A. Guerra, L. Montañez, A. Winnacker, F. De Zela, and R. Weingärtner, "Thermal activation and temperature dependent PL and CL of Tb doped amorphous AlN and SiN thin films," *Phys. Status Solidi*, vol. 4, no. 8, p. n/a–n/a, 2015.

[74] G. Xu, P. Jing, M. Tazawa, and K. Yoshimura, "Optical investigation of silicon nitride thin films deposited by r.f. magnetron sputtering," *Thin Solid Films*, vol. 425, p. 196, 2003.

[75] E. Paule, E. Elizalde, J. M. Martínez-Duart, and J. M. Albella, "Optical properties nitride

films," vol. 37, pp. 395–397, 1987.

[76] S. García, J. M. Maŕtin, I. Mártil, and G. González-Díaz, "Optical characterization of silicon nitride films deposited by ECR-CVD," *Vacuum*, vol. 45, no. 10, pp. 1027–1028, 1994.

[77] M. S. Aida, a. Attaf, and M. L. Benkhedir, "The optical properties of sputtered amorphous silicon nitride films: Effect of RF power," *Philos. Mag. Part B*, vol. 73, no. March 2015, pp. 339–347, 1996.

[78] W. C. Tan, S. Kobayashi, T. Aoki, R. E. Johanson, and S. O. Kasap, "Optical properties of amorphous silicon nitride thin-films prepared by VHF-PECVD using silane and nitrogen," *J. Mater. Sci. Mater. Electron.*, vol. 20, no. SUPPL. 1, pp. 18–21, 2009.

[79] C. Ko, J. Joo, M. Han, B. Y. Park, J. H. Sok, and K. Park, "Annealing Effects on the Photoluminescence of Amorphous Silicon-Nitride Films," *J. Korean Phys. Soc.*, vol. 48, no. 6, pp. 1277–1280, 2006.

[80] S. V Deshpande, E. Gulari, S. W. Brown, and S. C. Rand, "Optical properties of silicon nitride films deposited by hot filament chemical vapor deposition," *J. Appl. Phys.*, vol. 77, no. 12, p. 6534, 1995.

[81] M. Vetter, "Surface passivation of silicon by rf magnetron-sputtered silicon nitride ® lms," *Thin Solid Films*, vol. 337, pp. 118–122, 1999.

[82] J. Xiaoyun, "Structure and Optical Characterization of Silicon Nitride Films Deposited By R . F . Magnetron Sputtering."